NTNU – Trondheim
Norwegian University of
Science and Technology

Link Budget Parameters for CAMOS

Erik Fremming Aurbakken

Master of Science in Electronics
Submission date: Januar 2015
Supervisor: Torbjørn Ekman, IET
Co-supervisor: Roger Birkeland, IET

Norwegian University of Science and Technology
Department of Electronics and Telecommunications

Problem Description

The CAMOS project aims to design a remote sensor system that can be deployed in the Arctic area, here defined to be from the North Pole to 70 degrees North. This system will consist of deployed floating sensor nodes, submerged nodes, UAVs, AUVs and a satellite payload for transferring measured data to a data center. All nodes in the network will be interconnected through various communication networks. This assignment will study the data link between the node and the satellite.

In this project, the student should study the relationship and trade-offs related to CAMOS link budget parameters. The student should analyse how the choice of antennas and antenna diagrams and orbit parameters inflict on the total link budget, satellite footprint, revisit time and contact time for one node.

Main specification parameters: All nodes should have a revisit time by the satellite of less than 24 hours. The satellite should have an operational lifetime of 2 years (orbit lifetime of $>>$ 2 years). Different user cases and amounts of data transmitted from the nodes should be investigated and discussed.

Orbit simulations should be carried out by using Systems Tool Kit (STK).

Abstract

In the CAMOS project, a node network with sensors is proposed for research and monitoring in the Arctic zone. Today, there are large limitations for communication in the area. Different satellite systems do exist, but none are found to be suitable for the sensor network. A part of the CAMOS project is a new satellite communications system, customized for this use. This study concerns this satellite system, which has a primary area of target between Greenland to the west and Novaya Zemlya to the east. The latitudes of interest are 70°N and north to the North Pole.

Two types of orbits within LEO, a polar orbit with an elevation angle of 90° and a sun-synchronous orbit (SSO) with an elevation angle of 98°, have been compared with respect to coverage, connection time and revisit time. For the satellites used in the simulations, two different antennas were customized to fit hard cut-off Earth station elevation angles of 20° and 30°. Simulations in STK showed that a satellite in polar orbit had more passes with connection per day than in SSO at latitudes of 80°N and north, while a satellite in SSO had more at 72°N and 76°N. Up to eight more passes with connection were obtained using an elevation angle of 20°, than with 30°. While the polar orbit had connection with at least eight sensors for every pass, SSO had five consecutive passes without any connection for an elevation angle of 30°. A 20° elevation angle gave longer connection times than 30°, with most frequent time difference within the interval of 100 to 110 seconds.

A link budget has also been estimated for the two different antennas with three different data rates; 0.5, 1.0 and 1.5 kbit/s. The radiation patterns of the antennas were theoretical, and assumptions and other work have been used for parameters that could not be calculated. A link margin of 5 dB was required for the system. With a transmitted power from the transmitting antenna of 50 mW, only a data rate of 0.5 kbit/s and an antenna designed for 30° elevation angle met this requirement at the elevation angle limit, with 6.3 dB. An increase of the data rate from 0.5 kbit/s to 1.0 kbit/s resulted in a 3 dB decrease of the link margin, while an increase from 1.0 kbit/s to 1.5 kbit/s gave an additional decrease of 1.8 dB. The link margin cost of using an antenna customized for 20° compared to 30° was found to be 4.4 dB at the lowest elevation angle limits.

Sammendrag

I CAMOS-prosjektet er et nodenettverk med sensorer foreslått for forskning og overvåking i Arktis. I dag er det store begrensninger for kommunikasjon i området. Satellittsystemer eksisterer, men ingen har vist seg å være egnet for et sensornettverk. En del av CAMOS-prosjektet er et nytt satellittkommunikasjonssystem tilpasset for denne bruken, som denne oppgaven omhandler. Primærområdet av interesse er mellom Grønland i vest og Novaja Semlja i øst. Breddegradene av interesse er 70°N og nord til Nordpolen.

To typer lavbaner, en polar bane med inklinasjonsvinkel på 90° og en sol-synkron bane (SSO) med en inklinasjonsvinkel på 98°, har blitt sammenlignet med hensyn til dekning, tilkoblingstid og tiden mellom forbindelse. For satellittene som brukes i simuleringene ble to forskjellige antenner tilpasset jordstasjonens elevasjonsvinkler på 20° og 30°. Simuleringer i STK viste at en satellitt i polar bane hadde flere pass med tilkobling enn i SSO for breddegrader på 80°N og nordover, mens en satellitt i SSO hadde flere ved 72°N og 76°N. Med en 20° inklinasjonsvinkel var antallet pass med forbindelse opp til åtte ganger flere enn med 30°, per dag. Mens polar bane hadde forbindelse med minst åtte sensorer for hvert pass, hadde SSO fem sammenhengende pass uten forbindelse med noen noder med en elevasjonsvinkel på 30°. En 20° elevasjonsvinkel ga også lengre tilkoblingstider enn 30°, med hyppigste tidsforskjell innenfor intervallet 100-110 sekunder.

Et linkbudsjett har også blitt beregnet for de to forskjellige antennene med tre forskjellige overføringshastigheter; 0.5, 1.0 og 1.5 kbit/s. Antennenes strålingsdiagram var teoretiske, og forutsetninger og annet arbeid er blitt brukt for parametere som ikke kunne beregnes. En linkmargin på 5 dB har blitt satt som krav. Med en transmittert effekt på 50 mW fra antennen, møtte kun en overføringshastighet på 0.5 kbit/s og en antenne tilpasset for 30° kravet for marginen, med 6.3 dB. En økning fra 0.5 kbit/s til 1.0 kbit/s overføringshastighet ga en 3 dB redusering i linkmarginen, mens en økning fra 1.0 kbit/s til 1.5 kbit/s ga en ytterligere redusering p 1.8 dB. Kostnaden ved å bruke en elevasjonsvinkel på 20° i forhold til 30° var 4.4 dB på ytterpunktet for elevasjonsvinkelen.

Preface

This thesis is the final part of my Master of Science degree in Electronics at the Norwegian University of Science and Technology. It is part of the CAMOS project, a project within the Faculty of Information Technology, Mathematics and Electrical Engineering.

I would like to give a special thanks to Roger Birkeland, for helping me regularly throughout the last five months, by always being available for questions and comments. I would also like to thank Torbjörn Ekman for helping design the task. Finally, I would like to thank my fellow students for contributing to a good working environment, not only during this project, but throughout all my years at the university.

Erik Fremming Aurbakken Trondheim, January 16, 2015

Table of Contents

List of Figures

List of Tables

Abbreviations

A.N.	Ascending Node
ARGOS	Advanced Research and Global Observation Satellite
ASK	Amplitude Shift Keying
AUV	Autonomous Underwater Vehicle
AWGN	Additive White Gaussian Noise
BER	Bit Error Rate
BPSK	Binary Phase Shift Keying
CAMOS	Coastal and Marine Operation and Surveillance
DPSK	Differential Phase Shift Keying
EIRP	Effective Isotropic Radiated Power
FSK	Frequency Shift Keying
FSL	Free Space Loss
GEO	Geostationary Earth orbit
HEO	Highly Elliptical Orbit
HF	High Frequency
IADC	Inter-Agency Space Debris Coordination Committee
IME	Faculty of Information Technology, Mathematics and Electrical Engineering
INGV	Italian National Institute of Geophysics and Volcanology
ISO	International Organization for Standardization
ITU	International Telecommunication Union
LEO	Low Earth orbit
LNA	Low Noise Amplifier
MEO	Medium Earth Orbit
MF	Medium Frequency
NASA	National Aeronautics and Space Administration
NTNU	Norwegian University of Science and Technology
NPT	Norwegian Post and Telecommunications Authority
NUTS	NTNU Test Satellite
PFD	Power Flux Density
PLF	Polarization Loss Factor
PSK	Phase Shift Keying
QPSK	Quadrature Phase Shift Keying
RAAN	Right Ascension of the Ascending Node

SAR	Search and Rescue
SSO	Sun-Synchronous orbit
STK	Systems Tool Kit
TEC	Total Electron Content
UAV	Unmanned Aerial Vehicle
UHF	Ultra High Frequency
VHF	Very High Frequency

Nomenclature

a	Semi-major axis
A	Area
A_e	Effective area
b	Semi-minor axis
B	Bandwidth
B_E	Earth's magnetic field
BER	Bit Error Rate
c	Speed of light
C/N	Carrier to Noise ratio
d	Distance
e	Eccentricity
E_b	Bit energy
E_b/N_0	Energy per bit to noise power spectral density
EIRP	Effective isotropic radiated power
El	Elevation angle
f	Frequency
f_c	Carrier frequency
f_e	Flattening of an ellipse
f_E	Flattening of Earth
F	Power flux density (PFD)
FSL	Free space loss
g	Normalized gain to maximum gain
G	Gain
G_{max}	Maximum gain
G_r	Receiving antenna gain
G_t	Transmitting antenna gain
h	Height
i	Inclination
I	Intensity
k	Boltzmann's constant
L	Loss factor
L_{atm}	Atmospheric loss
L_{ion}	Ionospheric loss
L_{path}	Loss along the path

L_{pt}	Pointing loss
L_{RX}	Passive loss in receiving system
L_{trop}	Tropospheric loss
L_{TX}	Passive loss in transmitting system
LM	Link margin
n_e	Electron concentration
N	Noise power
N_0	Noise power spectral density
N_T	Total electron content
NF	Noise figure
P	Power
P_{fluc}	Fluctuation power due to scintillation
P_i	Incident power
P_{in}	Power fed to antenna
P_r	Received power
P_t	Transmitted power
PLF	Polarization loss factor
r	Radius
R_d	Data rate
R_E	Radius of Earth around equator
S_4	Ionospheric scintillation index
S/N	Signal-to-noise ratio
t	Time
t_o	Orbital period
t_{gt}	Group delay
T	Temperature
T_A	Antenna noise temperature
T_b	Brightness temperature
T_e	Equivalent noise temperature
T_i	Ambient temperature
T_S	System temperature
v	True anomaly
v_s	Satellite velocity
α	Angle from zenith in satellite
θ_B	Antenna beamwidth
θ_F	Faraday rotation angle
θ_{ps}	Phase shift angle
λ	Wavelength
μ	Standard gravitational parameter of Earth
ρ_a	Antenna aperture efficiency
Ψ_p	Angle between the polarization of an incident wave and the receiving antenna
ω	Argument of the perigee
ω_c	Carrier frequency ($\omega_c = 2\pi f_c$)
Ω	Right ascension of the ascending node (RAAN)
Ω_B	Solid angle

1 Introduction

The Coastal and Marine Operation and Surveillance (CAMOS) project is a lighthouse project within the Faculty of Information Technology, Mathematics and Electrical Engineering (IME) at the Norwegian University of Science and Technology (NTNU). In the project, a new satellite communication system for research and monitoring purposes in the Arctic is considered. A payload on board one of the NORSAT satellites is to be used to receive data from a network of low energy consuming sensors. This master's thesis investigates satellite coverage of the area of interest and gives an early stage prediction on the link budget.

1.1 Background

In the Arctic zone, here defined as north of $70°$N, including the ocean surrounding Svalbard, Norway, there has been an increase in activity, largely due to research. However, today, no good solution for communication in this area exists.

1.1.1 Communication issues in the Arctic

Some of the challenges for communication in the Arctic are the large distances and lacking infrastructure. Wired transmission with optical cables can be used, but these are expensive and economically inefficient. Wireless communications is therefore a better option. Due to the properties of the atmosphere, communication over large distances is possible. By using frequencies in the MF (300 kHz - 3 MHz) and HF (3 - 30 MHz) bands, which are used in maritime communications, a sufficient range is possible. However, the link quality for such systems depends on the weather, conditions, time and solar activity [3], and they are not suited for small antenna systems with a low power budget. The last option is satellite communications. Most satellite based communications systems use satellites in geostationary Earth orbit (GEO), orbiting above the equator, but due to the (nearly) spherical shape of the Earth, these satellites do not cover the entire Arctic zone. The theoretical limit is at $81.3°$N [4]. However, as the elevation angle for the Earth station goes towards zero as the latitude increases, the losses increase. This makes communication with GEO satellites almost impossible for small antenna systems north of $70°$N. Other types of satellite systems are therefore needed to get a good coverage of the Arctic zone. The same

applies in the southern hemisphere.

1.1.2 Existing and future systems

Systems with coverage of the Arctic do exist. An overview and evaluation of some of these is given in [5]. The two systems matching the requirements of CAMOS best are Iridium and ARGOS. However, ARGOS provides transmission of 32 - 256 bits, which is too low for the thought sensor network. Iridium can transmit more data, but it also requires a larger power for transmission from the nodes. In conclusion, none of the systems are likely to fit the sensor network.

An evaluation of future systems is also given in [5], coming to the same conclusion regarding the sensor network. One of the systems, however, is interesting and worth mentioning. This is the Arctic Satellite Communications project, which is a collaboration between the Norwegian Space Center, Telenor Satellite Broadcasting and SINTEF MARINTEK, but due to economical reasons, this project is uncertain [6]. Satellites in highly elliptical orbits (HEOs) are thought to be used for continuous broadband coverage. For the purpose of a power efficient sensor network, the distance to the satellites in HEO is too large. However, it is an interesting project parallel to CAMOS, which offers a smaller bandwidth.

1.2 The CAMOS project

At this stage, the goal of CAMOS is to propose a sensor network in the Arctic consisting of floating sensor nodes, submerged nodes, unmanned aerial vehicles (UAVs), autonomous underwater vehicles (AUVs) and one satellite for data transfer to the data center. Figure 1.1 shows the main area of interest, which is north of 70°N and between Greenland and Novaya Zemlya.

1.2.1 Specifications and considerations

Today, the project is in an early phase. An overview of some of the assumed details so far within the orbit selection and the uplink communication link are given here.

Orbit selection

Since GEO, which is the most common orbit for communications satellites, does not cover the entire Arctic, a different orbit is to be used. The two best fitting orbits in these areas are HEO and LEO (low Earth orbit), which both can be used with high inclination. By fully exploiting a HEO, only two satellites are needed for continuous coverage, but the distances are large, and for a low power budget sensor network, this is not efficient. A satellite system in HEO is also expensive, which is a big concern in the Arctic Satellite Communications project. A small satellite in LEO is cheaper and can have a high performance, as the early results from AISSat-1 have shown [7]. To get continuous coverage in LEO, several satellites are needed. However, in the CAMOS project, no real time data is required, and for now, only one satellite is considered.

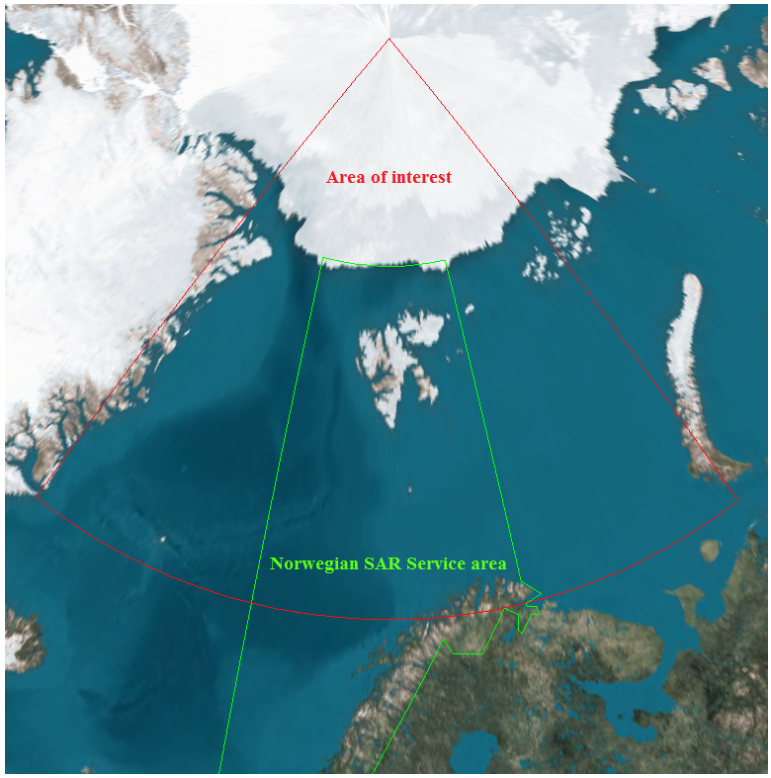

Figure 1.1: Area of interest in the CAMOS project and the Norwegian Search and Rescue Service area in the north [1].

Due to the low power budget, the distance to the satellite should be as small as possible. However, the orbit height also decides the lifetime of a satellite in it. This time is called orbital lifetime, and is defined as the time from the orbiting satellite's initial, to its demise or reentry into the Earth atmosphere. Millions of natural and artificial objects of varying sizes are orbiting around Earth. Examples are meteoroids, non-functional spacecrafts or satellites, abandoned launch vehicle stages and fragmentation pieces. These are called orbital debris, and spacecrafts and satellites are at risk of colliding with these. NASA is tracking more than half a million of the larger ($>$ 10 cm) pieces, but the rest are too small [8]. LEO is the region with most debris, and analysis indicates that collisions of debris larger than 10 cm will be the most dominant reason for more debris in the future [9]. Due to this, a recommendation of maximum time in an orbit is given. IADC has found 25 years to be a reasonable and appropriate lifetime limit for satellites in the LEO region [10]. For CAMOS, a minimum operational lifetime of two years has been set. However, the satellite will stay in orbit for a longer time. This time depends on different factors, such as satellite height, mass, drag area, drag coefficient and atmospheric density. Today, too little is known to estimate this lifetime, but it is assumed that a satellite height of 600 km will be within the recommendation. A height of 600 km is also believed to be low enough to get a communications link with low power.

Two different types of orbits at this height are discussed; polar orbit and sun-synchronous orbit (SSO). Both of these are good for the proposed system, but some differences are to be expected. According to Statsat, who is working on the NORSAT project, a launch into SSO is most likely [11], but potential advantages of a system in polar orbit are also investigated in this paper.

Link parameters

The use of radio frequency bands is regulated, and depends on the purpose of the system. For the CAMOS project, the purposes are both Earth exploration-satellite service and meteorological-satellite service. After consultation with the Norwegian Post and Telecommunications Authority[1] (NPT) suitable frequencies for the uplink from the sensor nodes to the satellite are 401 - 403 MHz [12]. Since work on this thesis started before NPT was contacted, a frequency of 400 MHz was assumed, and is therefore used.

Nothing is done so far with the hardware in the CAMOS system, and therefore the simulations are based on assumptions. The work here is based on an assumption that the transmitted power from the Earth station antenna (not the transmitter) is 50 mW. A lossless transmission between the transmitter and transmitting antenna is assumed, which in practice is not possible, but the losses in the system can be counteracted by higher transmitter power from the transmitter.

It is assumed that the needed data rate is 0.5 - 1.5 kbit/s, and the link budget is estimated for three different data rates in this range, 0.5, 1.0 and 1.5 kbit/s. The signal bandwidth is

[1] January 1st, 2015 the Norwegian Post and Telecommunications Authority was renamed the Norwegian Communications Authority.

set to 10 kHz, and a bit error rate of 10^{-3} is assumed.

A theoretical transmitting antenna radiating like a hemisphere, i.e. having an antenna beamwidth of 180°, is investigated. The antenna in the satellite has a beamwidth of 131.2°, which covers the entire area of Earth that can be seen from the satellite. These large beamwidths are used for getting a full overview over the connection at different elevation angles, and how this angle affects the link budget. Since the area of interest covers land, ice and water, different motions of the sensors are expected. For floating buoys, sea waves will affect the position and direction of the nodes. This is briefly discussed, but is not considered in the simulations.

1.2.2 Potential applications

By using a network of nodes, several areas of research and monitoring can be covered. In [13], some potential applications are listed. They are:

- Weather and climate measurements, e.g. wind, precipitation, pressure, salinity of water and temperatures.
- Pollution monitoring, e.g. oil spill.
- Mapping of biomass and marine resources.
- Animal tracking.
- Ice drift tracking.

Some of these, mainly the weather measurements, can provide important information for the Norwegian Search and Rescue (SAR) Service. Information about the weather and conditions can be crucial in a rescue operation. An approximate area served by the Norwegian SAR Service in the north is shown in green in Figure 1.1.

1.3 Thesis outline

In Chapter 2, theory related to orbits is presented. This includes the basic Keplerian elements and laws for defining orbits, and other parameters that must be considered when designing a satellite system. A brief description of different orbit types is also given. The simulation is described in Chapter 4. Results from the simulation are also presented, before they are discussed.

Propagation theory is presented in Chapter 3. The topics covered are antenna parameters, system and propagation losses and other parameters needed in the link budget. In Chapter 5 the link budget is given, where the theory from Chapter 3 is used to get a final link margin for the different system specifications. The results are then further discussed.

In Chapter 6 the work from this thesis is concluded. Some recommendations on further work are also given.

2 Orbit theory

Designing a satellite system requires detailed investigations of different scenarios. One major part is the choice of orbit. Height, orientation and shape of the orbit are some of the parameters needed to get a system to perform as desired. This chapter will give an introduction to these basic parameters and classify some orbits. A satellite system orbiting the Earth will be used, but the same theory applies for any body orbiting another body.

2.1 The orbit

The German scientist Johannes Kepler described planetary motion with three laws and six elements. With help from this, an orbit with a satellite can be fully defined. In this section these laws and elements are introduced.

2.1.1 Kepler's laws

Kepler formulated three laws explaining the motion of a body orbiting another body [14]:

1. An orbit around Earth is an ellipse, with Earth in one of the two foci (see Figure 2.1). The characterization of the ellipse is given by its semi-major axis a and eccentricity e. (These parameters are further explained in Section 2.1.2).

2. The area covered by the line between the Earth's centre and the satellite is equal for equal time intervals.

3. The cube of the semi-major axis is proportional to the square of the orbital period of any satellite in an elliptical orbit.

These can also explain how a satellite orbits the Earth.

2.1.2 The Keplerian elements

As mentioned, six elements are needed to fully define an orbit. These are called the Keplerian elements and give the shape, size and orientation of the orbit, and also the position of a satellite in it. Table 2.1 lists the elements, and they are shown in Figure 2.1 and 2.2.

Table 2.1: The six Keplerian elements.

Element	Description
a	Semi-major axis
e	Eccentricity
i	Inclination
Ω	Right ascension of the ascending node (RAAN)
ω	Argument of the perigee
v	True anomaly

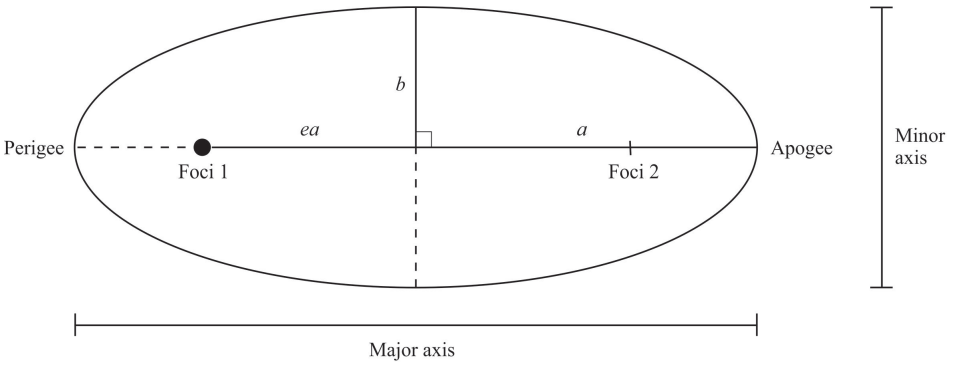

Figure 2.1: Ellipse with semi-major axis and semi-minor axis. Perigee and apogee are based on that Earth is in foci 1.

The shape of an ellipse is given by the semi-major axis a, half of the longest diameter, and semi-minor axis b, half of the shortest diameter. These are shown in Figure 2.1, and the semi-major axis is given by

$$a = \frac{\text{perigee} + \text{apogee}}{2}, \tag{2.1}$$

where perigee is the point on the orbit that is nearest to center of the Earth, and apogee is the furthest point. For a circle, the perigee and apogee will be of equal length, and the semi-major axis is the radius r of the orbit.

The eccentricity e defines the relation between the semi-major axis and the semi-minor axis. This is given by [14]

$$e = \frac{\text{apogee} - \text{perigee}}{\text{apogee} + \text{perigee}} = \frac{\text{apogee} - \text{perigee}}{2a} = \sqrt{\frac{a^2 - b^2}{a}}. \tag{2.2}$$

Due to the eccentricity, the semi-minor axis b is not needed to define an ellipse, and is therefore not one of the Keplerian elements. Table 2.2 lists the different types of shapes for different values of e.

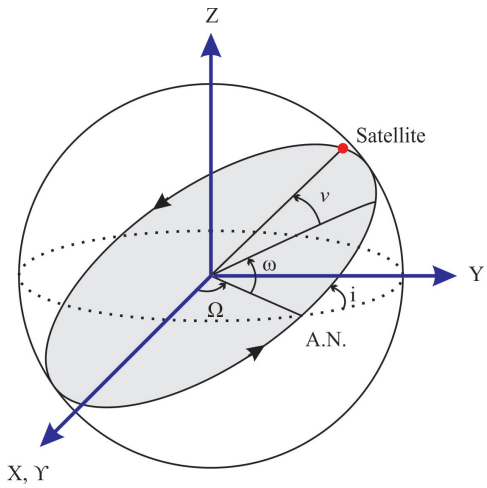

Figure 2.2: Keplerian elements related to the orbital plane and the reference plane.

Table 2.2: Different shapes depending on the eccentricity.

Parameter	Shape
$e > 1$	Hyperbola
$e = 1$	Parabola
$e < 1$	Ellipse
$e = 0$	Circle

The inclination i is one of the elements describing the orientation of the orbital plane. It is the angle between the Earth's equatorial plane and the orbital plane as shown in Figure 2.2, and can be in the interval of 0 - 180°. The inclination also gives the highest latitude of which the satellite passes over, e.g. a satellite with $i = 70°$ (or $i = 180° - 70° = 110°$) will never pass north of 70°N.

In Figure 2.2, the only reference is X, which is in the direction of the vernal equinox Υ. Y is perpendicular to X along equator, while Z is perpendicular to X and Y, increasing in the northern hemisphere. Related to the direction of vernal equinox is the right ascension of the ascending node (RAAN) Ω. It also describes the orientation of the orbital plane, by giving the position of the satellite when passing the equator, ascending. This is given by the angle from the direction of vernal equinox to the ascending node (A.N.) along the horizontal plane, as can be seen in Figure 2.2. RAAN is in the interval of 0 - 360°.

The location of the major axis is defined by the argument of perigee ω. It is given by the angle from A.N. to the line between Earth and perigee, in the same direction as the

satellite orbits. The argument of perigee is in the interval of 0 - 360°.

True anomaly v describes where the satellite is in the orbit, and is the only time dependent element. It is given by the angle from the argument of perigee to the line between the Earth and the satellite. The true anomaly is also in the interval of 0 - 360°.

2.2 Satellite specification

Now, as the orbit is defined, some properties of a satellite in the orbit will be introduced. These include height, period, satellite velocity and revisit time.

2.2.1 Height

The height h of a satellite in orbit is the distance from the satellite to the surface of Earth. For a circular orbit this is given by

$$h = a - R_E = r - R_E, \tag{2.3}$$

where r is the orbit's radius, and R_E is the radius of Earth. The radius used here, is the radius around equator, and is 6378.14 km.

2.2.2 Orbital velocity and period

For a satellite to stay in orbit at a certain height, a certain velocity v_s is needed. This is given by [14]

$$v_s = \sqrt{\mu \left(\frac{2}{d} - \frac{1}{a} \right)}, \tag{2.4}$$

where d is the distance from a satellite in orbit to the centre of Earth and μ the standard gravitational parameter. For Earth, $\mu = 3.986013 \times 10^5$ km^3/s^2. In a circular orbit, $d = a = r$ at all times, and Equation 2.4 can be rewritten as

$$v_s = \sqrt{\frac{\mu}{r}}. \tag{2.5}$$

The orbital period t_o is the time a satellite uses to make one revolution around Earth. It follows Kepler's third law, and is given by [14]

$$T = \frac{2\pi a^{3/2}}{\sqrt{\mu}}. \tag{2.6}$$

As can be seen, this time only depends on the semi-major axis. Again, for a circular orbit, $a = r$.

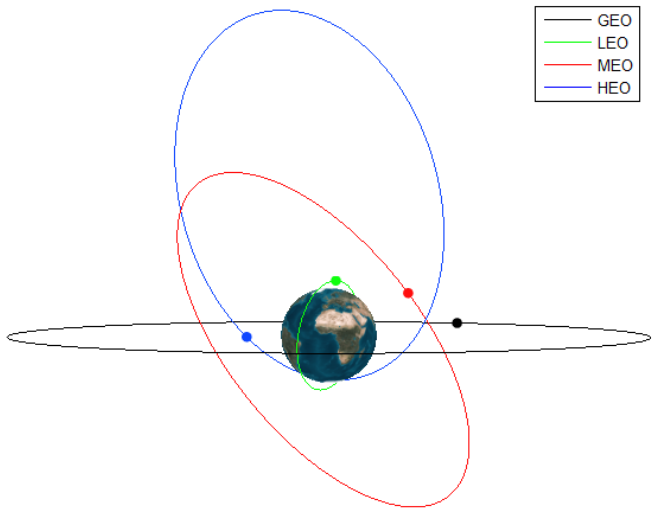

Figure 2.3: Examples of satellites in different types of orbits.

2.2.3 Revisit time

Revisit time is the elapsed time between connections between a stationary Earth station and a satellite. The shortest revisit time occurs when an Earth station has connection with the satellite in two consecutive revolutions.

2.3 Types of orbits

This section gives a short introduction to four types of orbits, depending on the values of the elements defined in Section 2.1.2. Examples of satellites in these different orbits can be seen in Figure 2.3. In the end, two orbits within the low Earth orbit type are defined.

2.3.1 Geostationary Earth orbit

Geostationary Earth orbit (GEO) is the most common orbit for communications satellites. A satellite in this orbit will have a revolution period of 23 hours and 56 minutes, the same as the Earth's rotation period. In addition, the orbit is circular and is in the equatorial plane [15]. This makes the satellite appear motionless above the equator. With a height of around 36 000 km, the satellite has a large coverage area, around 43% of Earth [14]. However, at high latitudes, the elevation angle is low. Its theoretical northern limit is at 81.3°N, but at around 70°N, the elevation angle is only 11 - 12°. At such low elevation angles, the attenuation is large. The same applies on the southern hemisphere. As mentioned, the long path length provides a large coverage area, but it leads to disadvantages, such as a large path loss and time delay when communicating with Earth.

2.3.2 Low Earth orbit

Low Earth orbit (LEO) satellites are orbiting the Earth in near circular orbits with heights of typically 200 - 2000 km. The short distance from Earth makes the time delay and path losses smaller compared to a GEO satellite. Hence, antenna systems can be smaller, and lower transmission power is required. Inserting a satellite in this orbit requires less energy, thus the life cycle cost may be lower. However, the low height also has some shortcomings. The coverage from one satellite is small, only 1.5 - 12% (depending on height [14]) of Earth, and a constellation of several satellites is needed to operate with continuous coverage. Seen from a fixed location on Earth, one satellite is only visible for around 8 to 10 minutes. One revolution around the Earth takes 88 - 120 minutes depending on the height [15].

2.3.3 Medium Earth orbit

In between LEO and GEO is the medium Earth orbit (MEO). The typical height here is around 10 000 km to 20 000 km. In this orbit, the disadvantages mentioned for LEO and GEO are reduced, but at the same time, some of the advantages are also reduced. Satellites for remote sensing, meteorological and positioning often use MEO. An Earth terminal has contact with an satellite in MEO for about one to two hours per pass [15].

2.3.4 Highly elliptical orbit

Highly elliptical orbits (HEO) have high eccentricity, i.e. a large difference in distances to perigee and apogee. A perigee height of around 1000 km and a apogee height of around 40 000 km is typical. The orbit is used to provide coverage in areas of high latitudes, not reached by satellite in GEO, but has a longer dwell time than satellites in LEO [15]. As the apogee height is larger than the perigee height, a satellite will stay longer above the designated area, which can be explained from Kepler's second law, defined in Section 2.1.1. The Molniya orbit is the most used HEO for communication purposes, and is the one showed in Figure 2.3.

2.3.5 Polar orbit

A polar orbit is an orbit where the satellite passes above the poles in every revolution, i.e. the inclination is close to 90°. Because of the rotation of the Earth, the satellite passes equator to the west of the last revolution. The polar orbit uses LEO, and can be used to gather data, since it covers the entire Earth on a periodic cycle [15]. In Figure 2.3, the LEO is a polar orbit.

2.3.6 Sun-synchronous orbit

Another special orbit within LEO is the sun-synchronous orbit (SSO). For SSO, the angle between the orbital plane and the Earth-sun line is constant. Consequently, every time the satellite passes over a given location, the local solar time is the same [14]. For this to occur, a specific inclination is needed. This inclination depends on the orbit height, and is shown in [16]. For heights of 400 - 1500 km, the inclination is 97 - 102°.

3 Propagation Theory

This chapter gives an introduction to the theory of electromagnetic waves from a transmitter to a receiver via the antennas and the atmosphere. Since CAMOS will use a frequency of around 400 MHz, the main focus is in the Ultra High Frequency (UHF) band.

3.1 Antenna parameters

In the transmitting end, an antenna converts electric power to radiowaves before the wave propagates through space, and vice versa in the receiving end. This section will explain some basics on antennas needed for making a link budget.

3.1.1 Gain and EIRP

Starting with a theoretical isotropic antenna, i.e. an antenna radiating the power P_t uniformly in all directions, power flux density (PFD) can be defined. If the antenna is placed in the center of an imaginary sphere with radius r, the power flux density F at the sphere is measured in Watts per square meter and is given by [17]

$$F = \frac{P_t}{4\pi r^2}. \tag{3.1}$$

For a satellite antenna there is no point of radiating in all directions. A satellite used for communications with Earth will use a directive antenna to concentrate the radiated power towards the intended area. The antenna gain G is the ratio of PFD radiated by a directive antenna to the PFD radiated by an isotropic antenna with same input power and is dimensionless. Thus, the gain will depend on the direction given by azimuth θ and elevation ϕ. It can be expressed by

$$G(\theta, \phi) = \frac{P(\theta, \phi)}{P_{in}/4\pi}. \tag{3.2}$$

Here, $P(\theta, \phi)$ is the power radiated by the antenna, while P_{in} is the power fed to the antenna. This equation does not consider losses in the antenna, which lead to a decrease in the effective area A_e. The effective area depends on the physical area of the antenna A and the antenna aperture efficiency ρ_a.

$$A_e = \rho_a A. \tag{3.3}$$

This effective aperture is related to the gain by [17]

$$G = \frac{4\pi A_e}{\lambda^2}, \tag{3.4}$$

where λ is the wavelength given by $\lambda = c/f$, c being speed of light (299792458 m/s) and f the frequency.

Another way of representing the transmitted power and gain is with the effective isotropic radiated power (*EIRP*). This is given by the product of them.

$$\mathit{EIRP} = P_t G_t. \tag{3.5}$$

In decibel, this is given by

$$\mathit{EIRP} = P_t + G_t, \tag{3.6}$$

where the unit for P_t is dBW and for G_t is dBi.

3.1.2 Beamwidth and directivity gain

The gain depends on the direction, as can be seen in Equation 3.2. When the gain is plotted as a function of θ and ϕ, the radiation pattern is obtained. The radiation pattern is normalized to maximum gain G_{max}:

$$g(\theta, \phi) = \frac{G(\theta, \phi)}{G_{max}}. \tag{3.7}$$

The main lobe is in the direction of maximum gain, called boresight. Side lobes will also occur, and these have lower gain. Usually, when designing an antenna, the goal is to maximize the main lobe and minimize the side lobes as much as possible. An example of a radiation pattern is shown in Figure 3.1. The antenna beamwidth is found by looking at the main lobe, and defined as the angle between two directions where the power density holds a certain value. A well known definition is the -3 dB beamwidth, which is marked in the figure. Further in this paper, the beamwidth θ_B means the -3 dB beamwidth.

The gain is also related to the beamwidth. For an isotropic antenna all of the power is radiated uniformly in all directions, i.e. the gain is 1 (0 dB). When the beamwidth of radiation is smaller, the radiated power is concentrated and the gain is given by

$$G(\theta, \phi) = \frac{4\pi}{\Omega_B}, \tag{3.8}$$

where Ω_B is the solid angle in steradians, given by

$$\Omega_B = \iint_S \sin(\theta)\, \mathrm{d}\theta\, \mathrm{d}\phi. \tag{3.9}$$

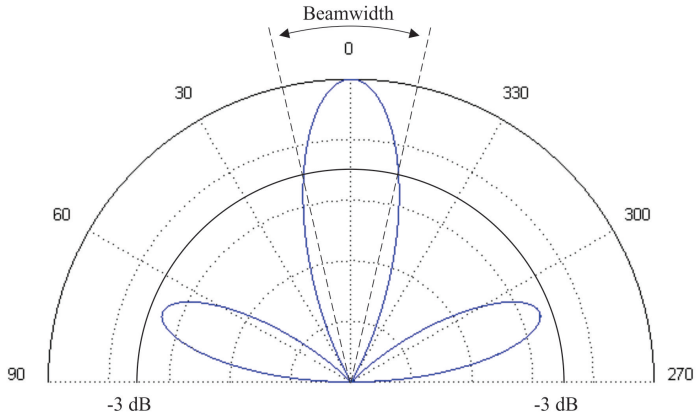

Figure 3.1: Simple radiation pattern showing the -3 dB beamwidth.

3.1.3 Polarization

The polarization is defined by the orientation of the electric field of an electromagnetic wave. Polarization is usually classified into linear, circular and elliptical polarization. However, both linear and circular polarization are special cases of elliptical polarization. For linear polarization, the electric field vector lies in a plane and the direction of resultant vector is constant with respect to time. The two perpendicular electric field vector components are in phase. This plane is either horizontal (horizontally polarized), vertical (vertically polarized), or inclined (slant polarization) which has horizontal and vertical components. If the two electric field vector components are not in phase, it is elliptical polarization with two orthogonal linearly polarized components. When these components have equal magnitude, it is circular polarization.

3.2 Atmospheric propagation effects

The path of the propagating wave between a satellite and an Earth station passes through the atmosphere. This results in a reduction in the quality of the signal. Variations in signal amplitude, phase, polarization and angle of arrival are all dependant on the frequency of operation, local climatology, local geography, type of transmission and elevation angle to the satellite [15]. Commonly, the atmosphere is considered to consist of the troposphere and stratosphere. Here, also the ionosphere is considered as a part of the atmosphere, and the atmosphere is considered to be 1000 km thick. Figure 3.2 shows the atmosphere, including some layers within the ionosphere. The layers merge into one another, so the figure shows approximate heights. Especially the troposphere and ionosphere result in reduction of the signal properties for a wave propagating through theses layers. Some of these effects are discussed next.

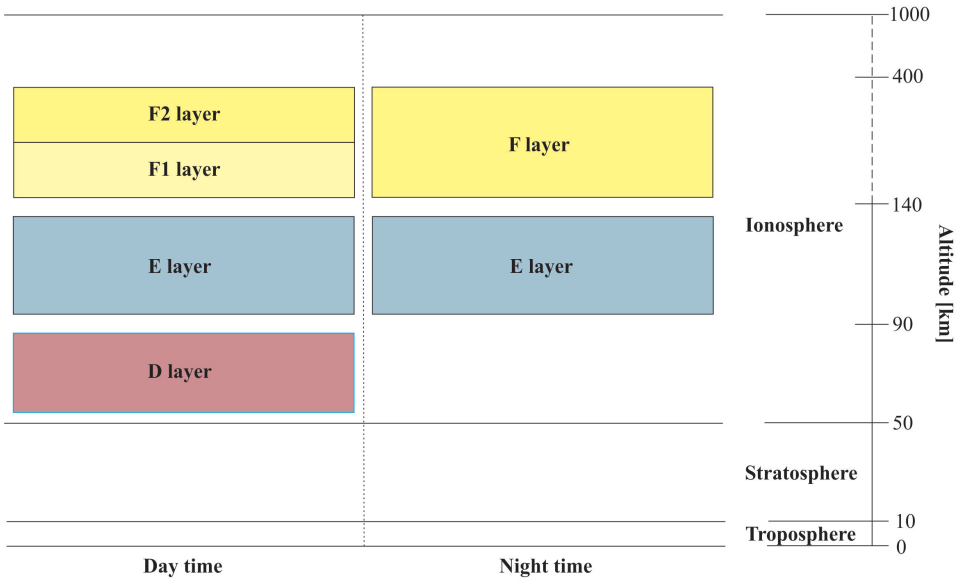

Figure 3.2: Layers of the atmosphere.

3.2.1 Tropospheric effects

The troposphere is the lowermost layer extending from the Earth's surface to 7 - 18 km depending on latitude and season. Most of the total mass of the Earth's atmosphere (70 - 80%) and most of the atmospheric water vapour (99%) is is contained in the troposphere [18]. This makes it important to investigate this layer, since the wave has to propagate through it. Here, some of the effects from the troposphere are introduced.

Electron absorption

For frequencies below 500 MHz, electron absorption is significant [14]. Absorption is a phenomenon that occurs due to interactions between the electromagnetic wave and free electrons in the troposphere.

The path through the troposphere increases for decreasing elevation angle El, and the loss due to absorption increases. The absorption loss for a certain elevation angle can be estimated based on the vertical loss $L_{atm,90^\circ}$, and is given by [14]

$$L_{atm} = L_{atm,90^\circ} \frac{1}{\sin(El)}. \tag{3.10}$$

Gaseous absorption

When the wave propagates through the troposphere, electromagnetic energy is absorbed due to the presence of molecular oxygen, atmospheric nitrogen and condensed water.

While the absorption due to molecular oxygen and condensed water is significant at frequencies between 1 and 15 GHz, the nitrogen absorption has its peak at around 300 GHz [14]. Losses due to gaseous absorption are reasonably predictable and can be approximated. Correction of losses due to elevation angle can be performed using Equation 3.10.

Attenuation due to precipitation and clouds

Losses due to different kinds of precipitation, e.g. rain and snow are far less predictable. The attenuation increases with increasing frequency and is significant above 10 GHz. Precipitation also causes depolarization of the signal. Circular polarized waves are more affected than linear polarized waves, and the effect is severe at frequencies above 15 GHz [14].

Cloud attenuation is significant for frequencies in Ka and V bands (27 - 75 GHz), but might also have some effect in L, S, C bands (1 - 8 GHz) and the Ku (12 - 18 GHz) band. The shape and content of liquid of the cloud and the elevation angle is influential to the attenuation. [14]

3.2.2 Ionospheric effects

The upper part of the Earth's atmosphere, the ionosphere, extends from about 15 - 50 km to 400 - 1000 km depending on literature [15] [19]. There are irregularities along the path, and gas molecules that release electrons due to the sun's radiation are present. The International Telecommunication Union (ITU) [20] states that these characteristics cause effects such as polarization rotation, refraction, dispersion, scintillation, group delay and absorption on Earth-space paths at frequencies between 100 MHz and 12 GHz. The most significant effects are introduced, but first the term total electron content is briefly explained.

Total electron content

The magnitude of some effects, e.g. polarization rotation and group delay in the ionosphere, is proportional to the total electron content (TEC). TEC gives the total number of electrons at a propagation path s (in meters) between two points with a cross section of one square meter. It is denoted N_T, and given by [20]

$$N_T = \int_s n_e(s)ds, \tag{3.11}$$

where n_e is the electron concentration in electrons per cubic meter. The TEC varies between 10^{16} and 10^{19} electrons per square meter, depending on time (diurnal, seasonal and solar cycle) and geographical location [20]. For propagation considerations, the ionosphere is divided into three layers (D, E and F), which have different densities of electrons. These layers can be seen in Figure 3.2. The F layer is the region with highest density of electrons, and is therefore the most significant layer. During the day, F is divided into F1 and F2, where F2 is the most significant [19].

Faraday rotation

Faraday rotation is rotation of polarization for a propagating wave due to interaction with the ionized medium in the Earth's magnetic field. The angle of this rotation θ_F (in radians) for a linearly polarized wave is proportional to the TEC. It also depends on the frequency f (in GHz) and the Earth's magnetic field B_E (in Teslas) [20].

$$\theta_F = 2.36 \times 10^{-14} \frac{B_E N_T}{f^2}. \tag{3.12}$$

Group delay and dispersion

Waves propagating through the ionosphere are delayed by charged particles. This time t_{gd} is called group delay. The phase of the signal is also advanced by the same amount. The group delay is given by [20]

$$t_{gd} = 1.345 \frac{N_T}{f^2} \times 10^{-7}, \tag{3.13}$$

where t_{gt} is in seconds.

For a signal with a broad bandwidth, dispersion should be considered due to the broad range of frequencies. As evident from Equation 3.13, the delay of a frequency component is inversely proportional to its frequency squared. Thus, higher frequencies are less delayed compared to lower frequencies. This differential delay is called dispersion, and should be taken into account for VHF and UHF when a broad bandwidth is used [20].

Scintillation

Irregularities in the ionosphere cause fluctuations of the refractive index, creating scintillations. This results in amplitude and phase fluctuations in the received signal, and can occur for frequencies up to 10 GHz. The scintillation index S_4 describes the intensity of these fluctuations and is expressed by [20]

$$S_4 = \left(\frac{\langle I^2 \rangle - \langle I \rangle^2}{\langle I \rangle^2} \right)^{1/2}, \tag{3.14}$$

where I denotes intensity and $\langle\rangle$ means averaging. This index can be weak ($S_4 < 0.3$), moderate ($0.3 < S_4 < 0.6$) or strong ($S_4 > 0.6$), and can be as high as 1.5. In weak regimes, the amplitude follows a log-normal distribution, while as S_4 approaches 1, the intensity follows a Rayleigh distribution. It is believed that S_4^2 is propotional to the secant of the zenith angles i_z up to $i_z \approx 70^\circ$ for weak and moderate scintillation. An empirical relationship between the scintillation index and the peak-to-peak fluctuations P_{fluc} is [20]

$$P_{fluc} = 27.5 S_4^{1.26}, \tag{3.15}$$

where P_{fluc} is in dB.

The occurrence of scintillations depends on the time. Typically, events occur after local ionospheric sunset and can last for hours. It is also seasonal dependant, and during maximum solar activity it occurs more often. Also the geographic location is influential. At mid-latitudes the scintillation is less intense than at high latitudes and near equator [20]. An illustration of the scintillation fading's time and location dependence is shown in [20] for a frequency of 1.5 GHz.

Absorption

Absorption also takes place in the ionosphere. In the equatorial and mid-latitude region, this is significant for frequencies below 70 MHz. At higher latitudes this limit and the absorption increases. This happens during two phenomenons, polar cap and auroral events [20].

Auroral absorption occurs over a range of 10 - 20° latitude centred close to the maximum occurrence of visual aurorae. It is caused by an increased electron density in the D and E region. The duration of this absorption spans from minutes to a few hours [20].

An absorption event that lasts longer is polar cap absorption, and can last for days. It may occur at geomagnetic latitudes greater than 64° and is caused by ionization. The event occurs usually during maximum solar cycle, where there may be 10 - 12 events per year [20].

3.3 Link budget parameters

In this section, additional parameters needed to build a link budget are considered. These are parameters related to the transmission, noise, different losses and the final link margin.

3.3.1 Distance from the Earth station to the satellite

The distance from the Earth station to the satellite depends on the elevation angle. For an elevation angle of 90°, i.e. when the Earth station is on a straight line between the satellite and the center of Earth, the distance d is equal to the height h of orbit, as discussed in Section 2.2.1. However, for other elevation angles, the distance is longer. Having Figure 3.3, the first step is using the law of cosines.

$$(R_E + h)^2 = d^2 + R_E^2 - 2dR_E \cos(\psi). \tag{3.16}$$

From Figure 3.3 it is evident that $\psi = 90^\circ + El$ whenever the satellite can be seen from the Earth station. Since

$$cos(\psi) = cos(90^\circ + El) = -\sin(El), \tag{3.17}$$

Equation 3.16 can be written as

$$(R_E + h)^2 = d^2 + R_E^2 + 2dR_E \sin(El). \tag{3.18}$$

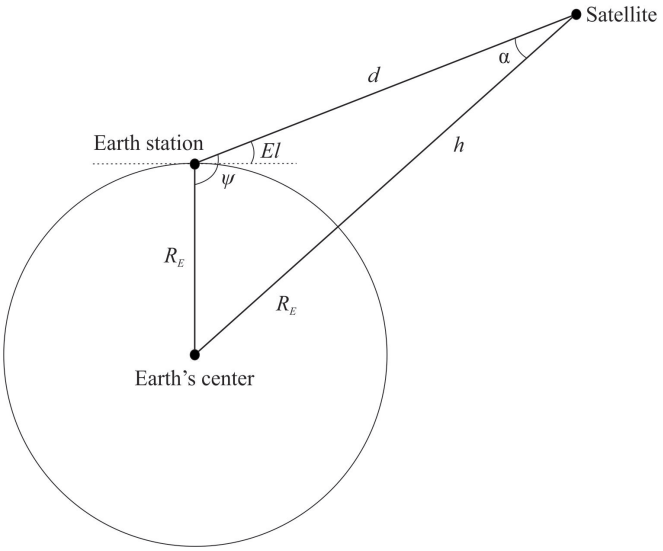

Figure 3.3: Elevation angle and distance geometry.

This can be rearranged to

$$d = \frac{-2R_E \sin(El) \pm \sqrt{(2R_E \sin(El))^2 - 4(R_E^2 - (R_E + h)^2)}}{2}, \tag{3.19}$$

which gives two values of d. Since this is an equation for distance, the answer has to be positive. By using minus, the answer will be negative for all elevation angles from $0°$ to $90°$. Therefore, the distance is given by

$$d = \frac{-2R_E \sin(El) + \sqrt{(2R_E \sin(El))^2 - 4(R_E^2 - (R_E + h)^2)}}{2}. \tag{3.20}$$

In this equation, it is assumed that the Earth is a perfect sphere, which it is not. The distance from the center of Earth to equator R_E is larger than the distance to the poles. Flattening f_e is a term describing this difference and is given by [21]

$$f_e = \frac{a - b}{a}, \tag{3.21}$$

where a is semi-major axis and b the semi-minor axis, both introduced in Section 2.1.2. The flattening of Earth is $1/298.257$. This gives a distance from Earth's center the poles of 6356.76 km. If the satellite orbit is circular and the height is set using R_E as reference, Equation 3.21 will not be correct for latitudes other than at equator. Further in this paper, this flattening is not accounted for, i.e. the Earth is assumed being a perfect sphere.

3.3.2 Free space loss

Free space loss, denoted *FSL*, is the power loss due to the distance between the transmitting and receiving antenna. It is inversely square proportional to the wavelength λ, i.e.

proportional to the frequency f squared, and is given by [14]

$$FSL = \left(\frac{4\pi d}{\lambda}\right)^2 \tag{3.22}$$

or

$$FSL = 20\log\left(\frac{4\pi d}{\lambda}\right) \tag{3.23}$$

in dB.

3.3.3 Antenna alignment

A satellite with a fixed antenna with boresight towards the center of Earth is assumed. The angle between the boresight and the actual direction of transmission path can be useful to calculate. If the beamwidth of the Earth station is known, it might be useful to have the relationship between this angle and the elevation angle, to decide what beamwidth on the satellite is needed. This relationship can also be used to calculate pointing loss, which is introduced in the next section. In Figure 3.3, this angle is denoted α, and can be calculated by using law of sines.

$$\frac{\sin(\alpha)}{R_E} = \frac{\sin(\psi)}{R_E + h}. \tag{3.24}$$

Since

$$\sin(\psi) = \sin(90^\circ + El) = \cos(El), \tag{3.25}$$

α is given by

$$\alpha = \sin^{-1}\left(\frac{R_E\cos(El)}{R_E + h}\right). \tag{3.26}$$

3.3.4 Pointing loss

To fully exploit the gain from the antennas, they have to be perfectly aligned with respect to the boresight. Using fixed antennas, antenna misalignment has to be considered. Misalignment leads to a decrease in the gain, which in a link budget is called pointing loss L_{pt}. This misalignment is shown in Figure 3.4 for the transmitting and receiving antenna, and the loss (in dB) can be calculated using [22]

$$L_{pt,TX} = 12\left(\frac{\theta_{TX}}{\theta_B}\right)^2 \tag{3.27a}$$

and

$$L_{pt,RX} = 12\left(\frac{\theta_{RX}}{\theta_B}\right)^2, \tag{3.27b}$$

respectively. For an Earth station antenna with boresight at 90° elevation angle, $\theta_{TX} = 90^\circ - El$, while for the antenna on the satellite $\theta_{RX} = \alpha$, assuming uplink. θ_B is the beamwidth of the respective antenna.

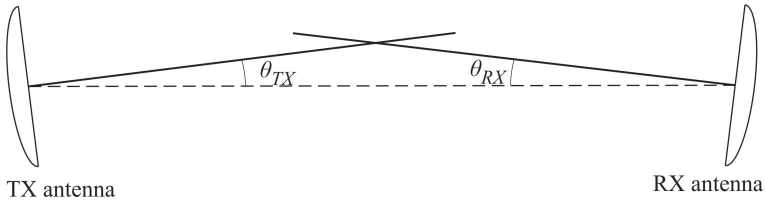

Figure 3.4: Antenna misalignment.

3.3.5 Polarization loss

As the radiowave propagates along the path through the atmosphere, the polarization of the signal will change. Faraday rotation is an example of an effect that affects the polarization, by causing the polarization of the wave to rotate. If the receiving antenna polarization is not oriented according to polarization of the incident wave, the receiver antenna will not receive at full power. This polarization loss is defined as polarization loss factor *PLF* and is given by

$$PLF = \frac{P_r}{P_i}, \tag{3.28}$$

where P_r is the power received by the antenna and P_i is the incident power. *PLF* is dimensionless and is between zero and one, where zero occurs when no power is received, while one means that all power is received. Since this power loss is due to polarization mismatch between the incident wave and the receiving antenna, the *PLF* for a linearly polarized wave can be expressed by the angle difference [23]

$$PLF = |cos(\Psi_p)|^2, \tag{3.29}$$

where Ψ_p is the angle between the polarization of the incident wave and the receiving antenna.

Combinations of different polarizations in the transmitter and receiver can also be used. Table 3.1 gives an overview of *PLF*s for different combinations of polarization for the incoming wave and the receiving antenna.

Table 3.1: Polarization loss for different combination of incoming wave and receiving antenna polarizations [2].

Polarization combination	*PLF* [dB]
Linear - linear	(0,∞)
Linear - circular	3
Circular - circular (same handedness)	0
Circular - circular (opposite handedness)	∞
Circular - elliptical (same handedness)	(0,3)
Circular - elliptical (opposite handedness)	(3,∞)

3.3.6 Passive system losses

In both the transmitter system and receiver system, passive losses (L_{TX} and L_{RX}), e.g. cable loss and impedance mismatch between the source and load, decrease the signal power. These losses can not be removed, but can be made small through optimization, by the use of optimized components.

3.3.7 Transmission equation

The power received in a communication link is the result of the transmission equation which is based on the Friis equation. The Friis equation assumes perfect conditions between two antennas and therefore, the only loss considered is free space loss. Based on the transmitted power and the gain of the two antennas, the received power P_r can then be estimated by [14]

$$P_r = P_t G_t G_r \left(\frac{\lambda}{4\pi d}\right)^2 \tag{3.30}$$

or

$$P_r = P_t + G_t + G_r + 20\log\left(\frac{\lambda}{4\pi d}\right) \tag{3.31}$$

in dB. By inverting the factor in the parenthesis in Equation 3.31, the last part is equal to free space loss. Further, the equation can be simplified by using $P_t + G_t = \textit{EIRP}$.

$$P_r = \textit{EIRP} + G_r - \textit{FSL}. \tag{3.32}$$

Other losses along the path can be included by modifying this equation. In this chapter several losses have been introduced. Together with free space loss (*FSL*), these are pointing losses ($L_{pt,TX}$, $L_{pt,RX}$), polarization loss (*PLF*) and atmospheric losses (L_{trop}, L_{ion}). The total loss along the path L_{path} can then be expressed as

$$L_{path} = \textit{FSL} + L_{pt,TX} + L_{pt,RX} + \textit{PLF} + L_{trop} + L_{ion}. \tag{3.33}$$

This gives a modified transmission equation,

$$P_r = \textit{EIRP} + G_r - L_{path}, \tag{3.34}$$

assuming perfect match between transmitter and transmitting antenna and between receiving antenna and receiver. However, as discussed in the last section, this is not possible. For estimation of the received power at the receiving antenna, the passive loss in the transmitting system (L_{TX}) then needs to be considered.

$$P_r = \textit{EIRP} + G_r - L_{path} - L_{TX}. \tag{3.35}$$

An estimation of received power at receiver also needs the passive loss in the receiving system (L_{RX}).

$$P_r = \textit{EIRP} + G_r - L_{path} - L_{TX} - L_{RX}. \tag{3.36}$$

3.3.8 Noise and temperature

Due to random motions of molecules, atoms and electrons, any component with a temperature of more than zero degree Kelvin, generates thermal noise power. This has large influence on the quality of the signal at the receiver. Here, some important terms about noise and temperature are introduced.

Noise figure and noise temperature

There are different ways of expressing the noise performance of a device. Noise figure *NF* is one way, and is defined as the ratio of signal to noise (S/N) power at a device's input to the S/N at its input [14]

$$NF = \frac{S_i/N_i}{S_o/N_o}. \tag{3.37}$$

A cascaded system with n devices with noise figure NF_1, NF_2, ... , NF_n will have a total noise figure of [14]

$$NF = NF_1 + \frac{NF_2 - 1}{G_1} + \frac{NF_3 - 1}{G_1 G_2} + \frac{NF_4 - 1}{G_1 G_2 G_3} + ... + \frac{NF_n - 1}{G_1 G_2 G_3 ... G_{n-1}}, \tag{3.38}$$

where G_1, G_2, ... , G_n denote the gain of the devices. For lossy devices $G = 1/L$, where L is the loss factor.

Another way of expressing the noise performance is the equivalent noise temperature T_e. A noisy component can be modelled as a noiseless device in series with a noisy resistor. The equivalent noise temperature is the temperature at which the resistor would generate the same noise power at the output of the ideal device, as that produced at the output by the actual device when terminated at its input by a noiseless resistance. It is given by [14]

$$T_e = T_i(NF - 1), \tag{3.39}$$

where T_i is the ambient temperature, often set to the standard temperature at Earth (290 K). In the case where the device is an attenuator and the ambient temperature is the same as that of the sourse resistance from which it is fed, the equivalent noise temperature can be defined as [14]

$$T_e = T_i(L - 1). \tag{3.40}$$

The equivalent noise temperature for a system with devices in cascade is found by [14]

$$T_e = T_1 + \frac{T_2}{G_1} + \frac{T_3}{G_1 G_2} + \frac{T_4}{G_1 G_2 G_3} + ... + \frac{T_n}{G_1 G_2 G_3 ... G_{n-1}}. \tag{3.41}$$

Antenna temperature

The antenna noise temperature is noise from radiating bodies within the radiation pattern. An antenna with gain $G(\theta, \phi)$ radiating in the direction (θ, ϕ) will pick up noise due to the brightness temperature $T_b(\theta, \phi)$ of a radiating body. Thus, the antenna noise temperature T_A (in Kelvin) is given by [22]

$$T_A = \frac{1}{4\pi} \int \int T_b(\theta, \phi) G(\theta, \phi) \sin(\theta) \, \mathrm{d}\theta \, \mathrm{d}\phi. \tag{3.42}$$

In the case of uplink, the noise for a receiving satellite antenna is from noise from outer space and noise from Earth. For downlink, a receiving antenna on Earth will get noise from the sky, as well as noise from the radiation of Earth.

The antenna noise depends on the elevation angle. Decreasing the elevation angle increases the antenna noise temperature caused by losses due to water and oxygen in the atmosphere [24].

System temperature

The total system temperature T_S can then be calculated by adding the equivalent noise temperature in the system with the antenna noise temperature,

$$T_S = T_e + T_A. \tag{3.43}$$

Thermal noise power

Thermal noise is power modelled as additive white Gaussian noise (AWGN). The noise power N is proportional to the temperature T and the bandwidth B of interest, and is given by

$$N = kTB, \tag{3.44}$$

where k is Boltzmann's constant defined as $k = 1.38 \times 10^{-23} J/K$.

The noise power spectral density N_0 is also proportional with the temperature and is given by

$$N_0 = \frac{N}{B} = kT, \tag{3.45}$$

where the unit for N_0 is W/Hz.

The noise power and noise power spectral density of a system is then given by inserting $T = T_s$ into Equation 3.44 and 3.45.

Carrier to noise ratio

The carrier to noise ratio C/N at the receiver is the ratio of the received carrier signal power to the received noise power and is given by

$$C/N = \frac{P_r}{N} \tag{3.46}$$

or

$$C/N = P_r - N \tag{3.47}$$

in dB.

3.3.9 Link quality

To be able to send baseband signals in a wireless communication link without large antennas, modulation is necessary. Modulation is a process in which a a carrier wave is created, including the signal. Amplitude shift keying (ASK), frequency shift keying (FSK) and phase shift keying (PSK) are three modulation schemes. In this paper, the link budget it based on PSK, and therefore only this scheme is further discussed.

PSK is a technique of varying the phase. The simplest form is called binary PSK (BPSK) where the carrier only assumes two different phase angles. These can be 0° and 180°, where for example the bit '0' corresponds to a phase shift of 0°, while the bit '1' corresponds to a phase shift of 180°. The carrier signal representing '0' and '1' can be expressed on a modulated cosine function as [14]

$$x_0(t) = A\cos(\omega_c t + \theta_{ps}) \tag{3.48a}$$

and

$$x_1(t) = -A\cos(\omega_c t + \theta_{ps}), \tag{3.48b}$$

respectively. ω_c denotes the carrier frequency ($\omega_c = 2\pi f_c$), t the time and θ_{ps} the phase shift angle.

Other forms of PSK can also be used. Examples are differential PSK (DPSK) and quadrature PSK (QPSK). Instead of BPSK, where each phase angle represent one bit, DPSK is based on the changes of the bit stream. If the bit stream changes, i.e. from 1 to 0 or from 0 to 1, '1' is transmitted, while '0' is transmitted if there is no change. QPSK is based on two BPSKs in quadrature. The bit stream is split in two. One of the bit streams then modulates a cosine function, while the other modulates a sine function. The vector sum of these orthogonal functions produces a QPSK signal given by [14]

$$x(t) = \cos[\omega_c t + \theta_{ps}(t)]. \tag{3.49}$$

Here, θ_{ps} can have four phase shift angles, 0°, 90°, 180° and 270°. Four different combinations with two bits can be transmitted, 00, 01, 10 and 11.

Closely related to the modulation scheme is the energy per bit to noise power spectral density ratio, denoted as E_b/N_0. As the name suggests, E_b is the energy each bit has (in Joule) and is given by the signal power, divided on the bit rate R_d (in bit/s). The energy per bit to noise power spectral density ratio in decibel is given by

$$E_b/N_0 = C/N + 10\log\left(\frac{B}{R_d}\right). \tag{3.50}$$

The link margin of the link is defined as the difference between the E_b/N_0 for the system and the required E_b/N_0. $E_b/N_{0,req}$ is given by the bit error rate *BER*, which sets a limit for the probability of a bit error. The relation between $E_b/N_{0,req}$ and the bit error rate is given by [15]

$$BER = \frac{1}{2}\text{erfc}\left(\sqrt{E_b/N_{0,req}}\right), \tag{3.51}$$

where the operator erfc() is the complementary error function, defined as [15]

$$\text{erfc}(x) = \frac{2}{\sqrt{\pi}}\int_x^\infty e^{-u^2}\,\mathrm{d}x. \tag{3.52}$$

The link margin *LM* is then given by

$$LM = E_b/N_0 - E_b/N_{0,req} \tag{3.53}$$

in dB, and describes how much additional attenuation the communication link can have, and still be working.

4 Orbit selection

In this section, the theory introduced in Chapter 2 is put in content with the CAMOS project. The inclination is one of the most important parameters for establishing the desired coverage, while the elevation angle should be set to cover as much as possible without decreasing other properties. First, the simulation is described, before results are presented and discussed.

4.1 Simulation

Before the results are presented, this section gives a brief introduction of the simulation tool. The input and setup for the simulation are also gone through.

4.1.1 Systems Tool Kit

Systems Tool Kit (STK) 10 is used to do simulations on the satellite system. The software can be used to analyse properties of a complete satellite system. So far in the CAMOS project, only the free version has been available. This limits the analysis, but the free version is sufficient for giving some early predictions. Some of the tools available in the free version are data on connection time, elevation angle and range.

4.1.2 Setup

The area of interest is shown in Figure 1.1. This area has been divided into 20 smaller areas with equal latitudinal and longitudinal size. One node is placed in each of these. The nodes can be seen in Figure 4.1 while their positions are given in Table 4.1. On each node *NXX*, a sensor (an antenna) *SXX* is placed. In the simulations, the sensors will radiate as simple conics with conic half angles of 70° and 60°, i.e. beamwidths of 140° and 120°. This corresponds to elevation angles from the Earth stations of 20° and 30°. The differences will be investigated and discussed. For the real system, a beamwidth of 180° will be used, but since the sensors will be floating on water, the waves will obscure the horizon. Another factor is that the propagation losses are higher for lower elevation angles, which will be discussed in Chapter 5.

Two satellites with different inclination, 90° and 98°, will be compared. Further, the orbit

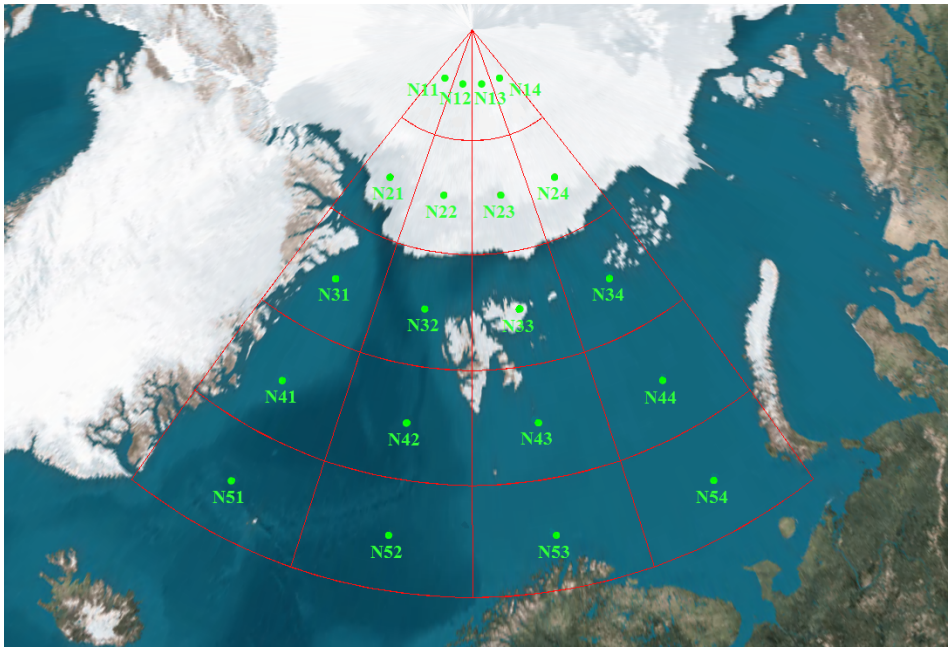

Figure 4.1: Placement of the nodes used in the simulation.

with inclination of $90°$ will be called polar orbit, while $98°$ is called sun-synchronous orbit (SSO). For an height of 600 km, $98°$ inclination is a bit too high for SSO. STK gives the inclination of 97.848 deg, however, in this paper it is considered sufficiently close. Table 4.2 lists the properties of the satellites. On both satellites, *Sat_i90* and *Sat_i98*, there is a sensor, *SSat_i90* and *SSat_i98*. These sensors are always directed towards the Earth, with boresight towards the Earth's center. In the simulations, these sensors radiate as a simple conic with a beamwidth $131.2°$, which cover 3.5% of Earth. This large angle is not needed since the end point will be outside the radiation of from the node sensors. Minimum required angles needed for elevations angels of $20°$ and $30°$ will be calculated later in this chapter.

The time used in the simulation is 22 Sep 2014 00:00:00.000 UTCG - 24 Sep 2014 00:00:00.000 UTCG. However, most of the results are based on the second day, while the first day is only used when the second day is insufficient.

Table 4.1: Positions of the nodes used in the simulation.

Node	Latitude [°N]	Longitude [°E]
N11	88	-12.5
N12	88	6.5
N13	88	25.5
N14	88	44.5
N21	84	-12.5
N22	84	6.5
N23	84	25.5
N24	84	44.5
N31	80	-12.5
N32	80	6.5
N33	80	25.5
N34	80	44.5
N41	76	-12.5
N42	76	6.5
N43	76	25.5
N44	76	44.5
N51	72	-12.5
N52	72	6.5
N53	72	25.5
N54	72	44.5

Table 4.2: Parameter of the satellites used in the simulation.

Satellite name	Semi major-axis a [km]	Eccentricity e	Inclination i [°]	RAAN Ω [°]
Sat_i90	6978.14	7.38839 $\times 10^{-16}$	90.0021	359.810
Sat_i98	6978.14	9.23549 $\times 10^{-16}$	98.0021	359.798

4.2 Results

In this section, the results from the simulations in STK are presented and discussed.

4.2.1 Passes

From the specifications for CAMOS in Section 1.2.1, a minimum of one pass with transmission of data every 24 hours is set. However, the goal is to optimize the system and get as many transmissions as possible. Here, the number of passes with connection between the satellites and the ground sensors are presented. In this simulation, only simulation for 24 hours is used (23 Sep 2014), to find the number of passes per day.

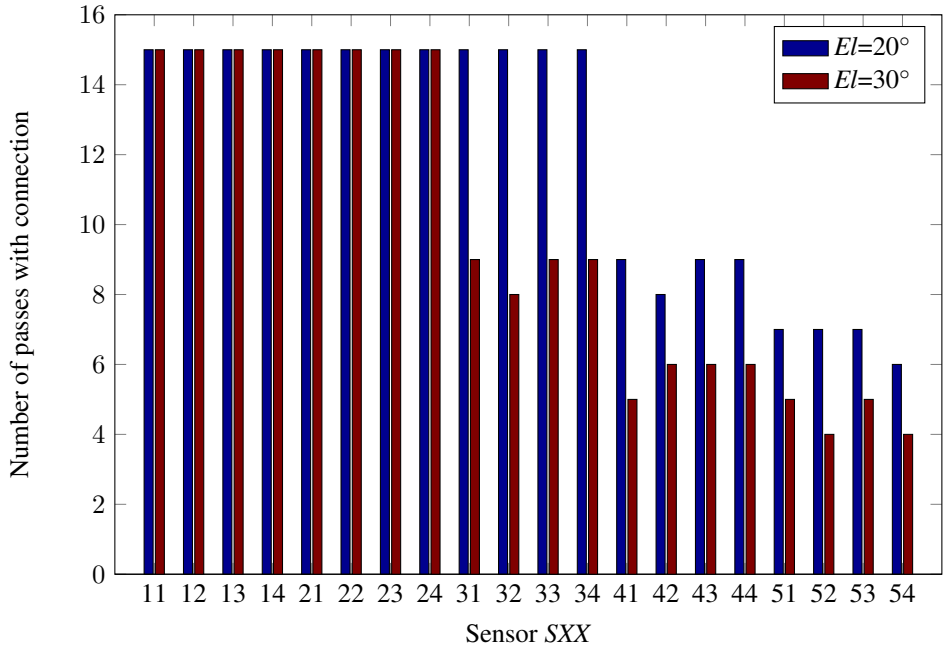

(a) Polar orbit.

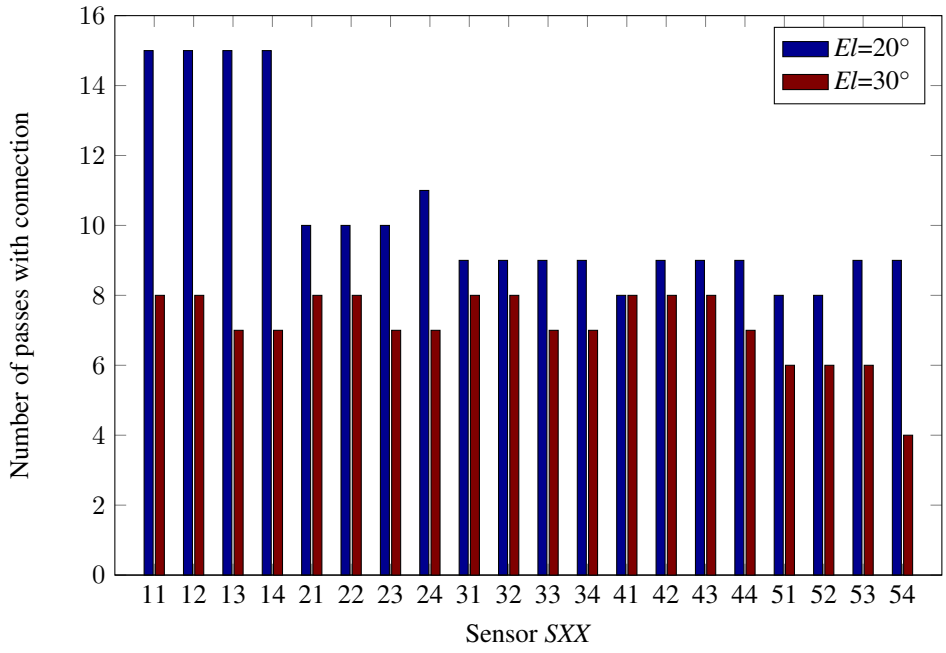

(b) Sun-synchronous orbit

Figure 4.2: Number of passes with connection for each sensor within one day (23 Sep 2014).

The total number of sweeps around the Earth only depends on the semi-major axis. For CAMOS, the orbit height is set to 600 km, which gives an semi-major axis of 6978.14 km. This corresponds to a satellite velocity of 7.6 km/s from Equation 2.5 and an orbital period of one hour, 36 minutes and 41 seconds from Equation 2.6. The total number of sweeps are then 14.9 within 24 hours, however, the satellites pass the area of interest 15 times in the simulation, i.e. 15 times is the maximum possible number of connections between the nodes and the satellites. In Figure 4.2 the total number of passes with connection for the nodes are shown for polar orbit (a) and SSO (b). For both values of inclinations, two different elevation angles for the nodes, 20° and 30° are shown. Further, a pass means a pass over the Arctic, not necessarily a pass over the area of the nodes.

By looking at Figure 4.2(a), where results for polar orbit are shown, it can be seen that at the latitudes 84°N and 88°N, every pass has connection to all of the nodes. At 80°N, only the elevation angle of 20° gives connection to all passes. An elevation angle of 30° gives eight or nine passes. The number decreases for decreasing latitude. 76°N gives eight or nine for $El = 20^\circ$ and five to six for $El = 30^\circ$. For the nodes lying longest south at 72°N, the numbers are six to seven and four to five, respectively.

For SSO, as shown in Figure 4.2(b), only an elevation angle of 20° gives connection during every pass at 88°N. Further, $El = 20^\circ$ gives ten to eleven passes with connection at 84° and eight to nine at 80°N, 76°N and 72°N. With an elevation angle of 30°, the results are more equal, with seven to eight sweeps at 88°N, 84°N, 80°N and 76°N. At 72°N the number is four to six.

4.2.2 Time with connection

In last section the number of passes with connection between the nodes to the satellites were discussed, but the connection time was not mentioned. It is assumed that 1.5 - 2.0 kbit of data is to be transferred for each node with connection, for each pass. The needed time for transfer is then 1 - 4 seconds, depending on the data rate (0.5, 1.0 or 1.5 kbit/s). In addition, some time is needed to ping the node and set up the link before it starts transmitting.

In Appendix A, Table A.5 - A.8 shows the times with connection for the different values of inclination and elevation angles for the 24 hours discussed. Mostly, the times range from about two-three minutes, but there are also some below one minute. For $El = 20^\circ$, the times can be as short as 40 - 50 seconds. The shortest times are down to around 16 seconds for $El = 30^\circ$. The elevation angle also has an impact on the longest times. For $El = 20^\circ$ the longest times with connection are around six minutes, while for $El = 30^\circ$ they are a little above four minutes. Generally, the times are a little longer for polar orbit than for SSO, although also the shortest times are with polar orbit.

4.2.3 Revisit time

The times between connection, called revisit times, are also investigated. The longest revisit times within 24 hours have been found. To do this the simulation time was 48 hours

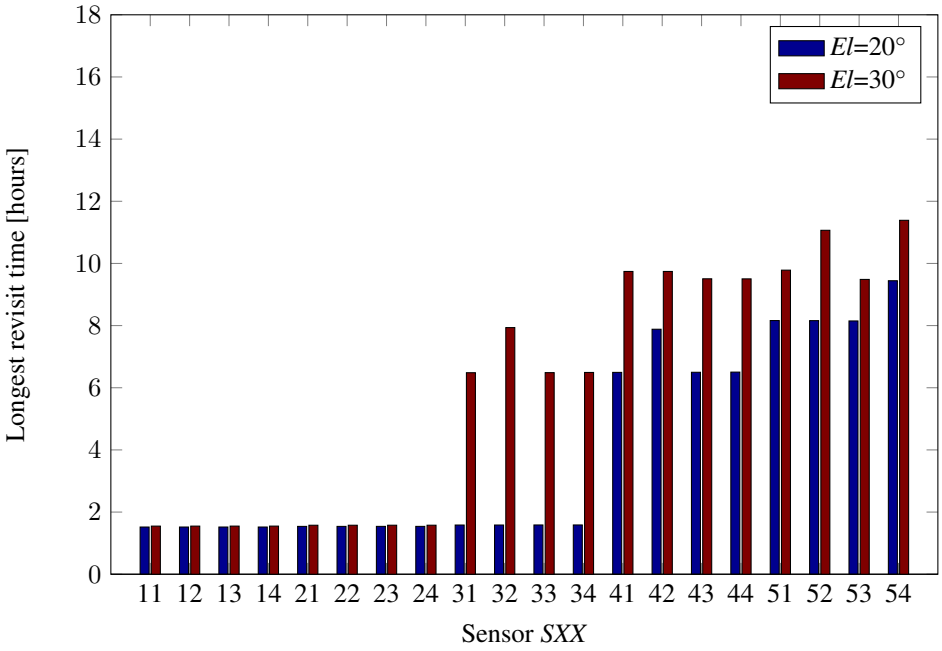

(a) Polar orbit.

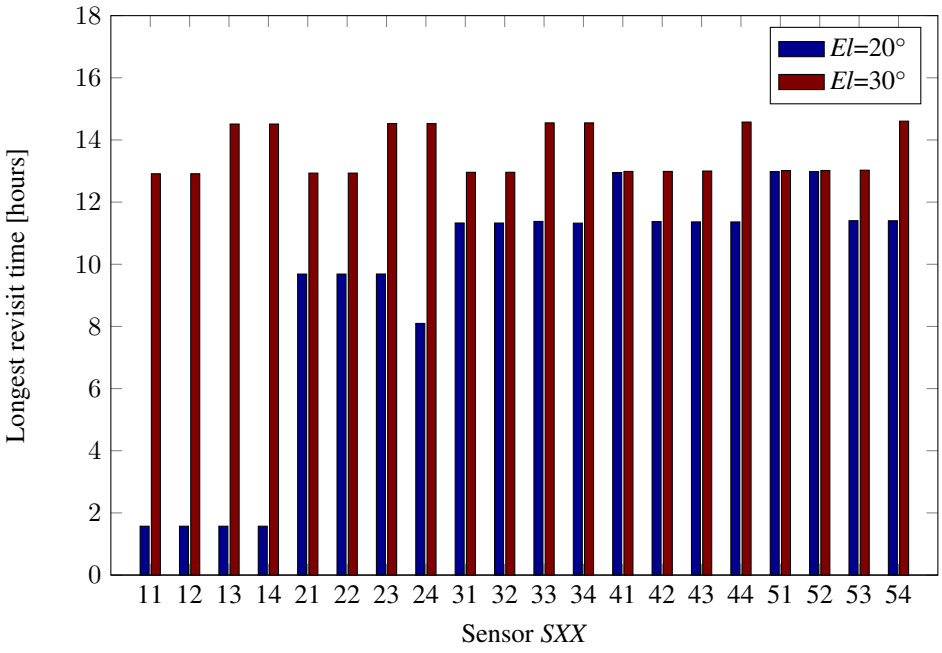

(b) Sun-synchronous orbit.

Figure 4.3: Longest revisit time for each sensor within 24 hours (23 - 24 Sep 2014).

(22 Sep 2014 and 23 Sep 2014). 23 Sep 2014 is the basis of the times, but if the first revolutions are without connection, data from 22 Sep 2014 have been used. Table A.1 - A.8 in Appendix A present the data for time per sweep, and also shows where there are revolutions with no connection. Figure 4.3 shows the longest revisit times for different elevation angles and inclinations. In Table A.9 and A.10 both the shortest and longest revisit times are given.

The longest revisit times for polar orbit are shown in Figure 4.3(a). An elevation angle of 20° gives the longest, of about 1.5 hours of revisit time, at 88°, 84° and 80° latitude. At 76° the sensors have the longest revisit times of around 6.5 to almost 8 hours, while the sensors at 72° have between a little more than 8 and almost 9.5 hours. With an elevation angle of 30° the times are around 1.5 hours at 88° and 84°. This increases to between 6.5 to almost 8 at 80°. At 76° and 72° they are about 9.5 hours, except for two sensors at 72° with a little more than 11 hours.

For SSO, as shown in Figure 4.3(b), only an elevation of 20° gives the longest revisit time of 1.5 hours at 88° latitude. At 84° this increases to between a little more than 8 to a little more than 9.5 hours. The three latitudes to the south (80°, 76° and 72°) have longest revisit times between 11 and 13 hours. With a 30° elevation angle the longest times are between almost 13 hours and around 14 hours for at all the simulated latitudes.

4.2.4 Minimum satellite beamwidth

Due to mismatch between the elevation angles of the nodes and the satellites, the beamwidth used on the satellite during the simulations (131.2°) is larger than what is needed. A smaller antenna (sensor) beam gives a more efficient antenna, which is desirable. By doubling the result from Equation 3.26 this minimum beamwidth has been found. For an elevation angle of 20°, this beamwidth is 118.4°, while it is 104.7° for an elevation angle of 30°.

4.3 Discussion

Results from two different elevation angles and two different orbits have now been presented. Here, the differences will be discussed and compared.

4.3.1 Elevation angles

From the results, it can be seen that an elevation angle of 20° gives higher or equal numbers of sweeps with connection than with 30°. The numbers presented in Figure 4.2, shows that up to eight passes more are obtained using 20°, compared to 30°. However, since the minimum required connection per day is set to be one, four passes per day, which is the lowest number of passes for $El = 30^\circ$, might be enough. In relation to this, a factor needs to be considered. In the simulation a hard cut-off at $El = 20^\circ$ and $El = 30^\circ$ is used. Since the transmitting antenna is assumed to have a beamwidth of 180°, this cut-off is due to the satellite antenna's beamwidth. In reality, a connection can be established outside

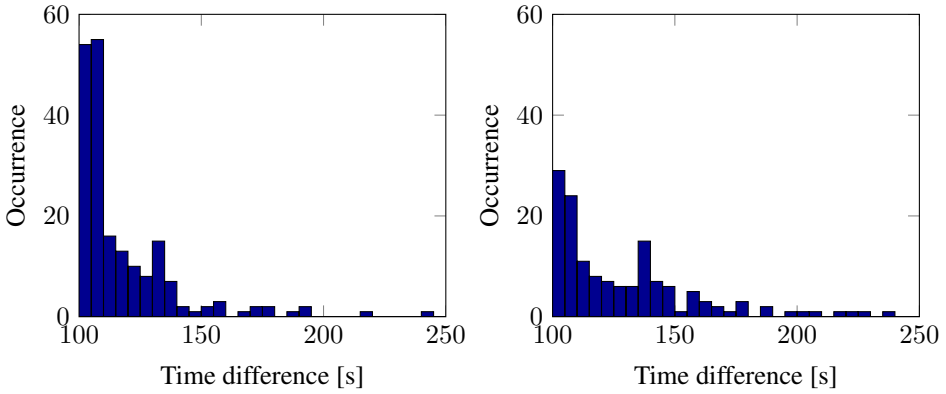

(a) Polar orbit.

(b) Sun-synchronous orbit.

Figure 4.4: Occurrence of connection time differences between elevation angles of 20° and 30°.

this, since this beamwidth is the -3 dB beamwidth. The signal will not be strong, but more passes with connection may appear.

An elevation angle of 20° will always result in a longer connection time than of 30°. The difference can be seen for each sensor in Table A.11 and A.12 in Appendix A, and is shown in Figure 4.4, using histograms. The width of each bar is five seconds, and it can be seen that a time difference of between 100 and 110 seconds occurs most frequently, meaning that most often, an extra connection time when using an elevation angle of 20° compared to 30° is within this interval. Assuming a small amount of nodes, this additional time might not be needed, and using 30° could be enough. However, if many nodes are close to each other, the total connection time on each node cannot be used. The satellite then needs to give each node a time for transmission. Another factor needing consideration is the sea waves the nodes will be exposed to. Large motion of these waves may cut the link, and the data might not be retransmitted. If this happens, a longer connection time is required. The shortest connection time is 16.1 seconds. This is probably too short to guarantee transfer of data, but if to be used, such a node would need priority for transmission, and having the whole time available. However, due to the assumption of hard cut-off, the connection times might be smaller than the times one could obtain in reality, and considering this, the short connection times might actually be long enough.

The revisit time is directly connected to the elevation angle, as evident from the results. Since the number of passes with connection depends on the elevation angle, a pass without connection will increase the revisit time significantly. A smaller difference also occurs since low elevation angle gives longer connection times, and therefore less time without connection. The lowest possible revisit time is around 1.5 hours, i.e. a little shorter than one revolution. The longest revisit times are a little more than 14.5 hours, which occur when the satellite makes eight consecutive passes without connection.

4.3.2 Orbits and latitudes

The results show that the difference between polar orbit and SSO are significant, especially at the highest latitudes. Since a satellite in polar orbit passes above the North Pole during every revolution, it covers the area from the North Pole and south to $84°$N in every pass, and even south to $80°$N with $El = 20°$. In SSO the satellite only covers nodes at $88°$N in every pass with the lowest elevation angle. The results show however, that with SSO, the number of passes are more even for all the nodes, and even better than the polar orbit at the lowest latitudes. Since the satellite never gets further north than $82°$ in SSO, there will be revolutions where it does not get contact with any of the nodes. Results from the simulation also show that this is reality for five consecutive passes. This gives a minimum of about 9.5 hours without connection to any of the nodes.

Today, the area which is in most need of a communications system is north of $80°$N. This is close to the theoretical limit for the satellites in GEO. The results show that for this area, the polar orbit is far better than the SSO with respect of numbers of passes with connection and revisit times.

5 Link budget

5.1 Results

Here, the different parameters and losses are quantified and presented. The final link budgets for the different combination are also given. In the end, it is all discussed. It should be noted that the values for the different elevation angles are related to the antenna matched to the intended elevation angle.

5.1.1 Parameters used

In Section 1.2.1 some values of parameters were given. These are listed in Table 5.1 and are the basic input data needed in the link budget. The frequency used is 400 MHz, and the orbit height is set to 600 km. In Table 5.1, the passive losses in the transmitter system are set to zero. This is not realistic, but is assumed to be counteracted by the transmitted power. Hence, the power transmitted from the transmitting antenna, is 50 mW. Link budgets for three data rates are to be investigated. These are 0.5, 1.0 and 1.5 kbit/s. Bandwidth is set to 10 kHz and the bit error rate is 10^{-3}.

Table 5.1: Parameters used.

Parameter	Description	Value	Unit
f	Frequency	400	[MHz]
h	Orbit height	600	[km]
P_t	Transmitting power from receiver	50	[mW]
L_{TX}	Passive losses in transmitter system	0	[dB]
R_d	Data rate	0.5, 1.0, 1.5	[kbit/s]
B	Bandwidth	10	[kHz]
BER	Bit Error Rate	10^{-3}	[-]

The transmitting antenna on the Earth station will have a beamwidth of $180°$ and using Equation 3.8 the gain is found to be 3 dBi. The power radiated from the antenna can then

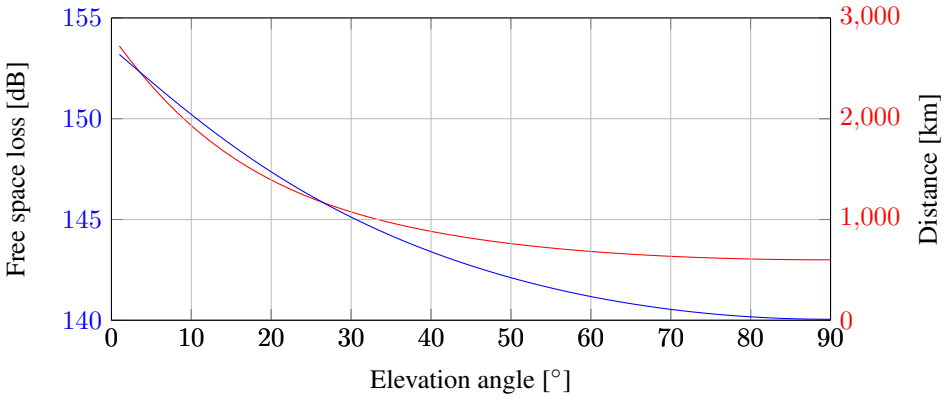

Figure 5.1: Free space loss and distance from Earth station to the satellite against the elevation angle.

be represented as *EIRP* and is given by Equation 3.6. With a transmitting power of 50 mW or 17.0 dBmW, the *EIRP* is 20.0 dBmW. The gain of the receiving satellite antenna also depends on the beamwidth. For the antenna matching an node elevation angle of $20°$, the beamwidth is $118.4°$ and the gain is 6.2 dBi. When the elevation angle is $30°$, the antenna has a beamwidth of $104.7°$, and a gain of 7.4 dBi. These antennas are highly theoretical and better than what can be expected in reality, but are used as a starting point, because choices regarding the antennas have not been made yet for the CAMOS project.

5.1.2 Losses

Free space loss

The largest loss in a satellite link is free space loss (*FSL*) due to the large distances. This loss can be estimated from Equation 3.23 and is shown in Figure 5.1 together with the distance between the Earth station and the satellite. Both are shown against the elevation angle for the Earth station. The three elevation angles of most interest, $90°$, $20°$ and $30°$, have distances of 600.0 km, 1392.4 km and 1075.2 km, respectively. Their associated free space losses are 140.1 dB, 147.4 dB and 145.1 dB.

Polarization loss

The polarization loss depends on the polarization of the two antennas. For a linear to linear combination it will be nearly impossible to estimate the polarization loss. From Equation 3.29 the effect from a rotated incident polarization versus the receiving antennas polarization can be calculated. However, at 400 MHz, Faraday rotation can cause rotations of $4.5 - 4500°$, depending on the electron concentration [20]. This makes estimating the polarization loss complicated, and therefore, a different combination of polarization is investigated. It is assumed that the Earth station antenna is linearly polarized, while the satellite antenna is circular. This gives a polarization loss factor of 3 dB as can be seen in

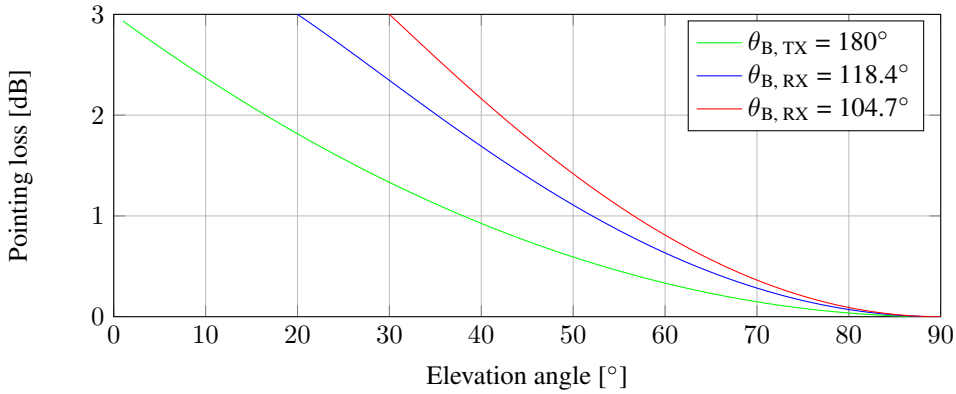

Figure 5.2: Pointing loss against the elevation angle for the three considered antennas.

Table 3.1.

Pointing losses

In Section 4.2.4 it was established that the needed satellite antenna beamwidth for an Earth station elevation angle of 20° and 30° is 118.4° and 104.7, respectively. These will have a boresight misalignment angle for elevation angles given in Equation 3.26. Using this and Equation 3.27, the pointing loss of the transmitting and receiving antenna can be found. Figure 5.2 shows the three pointing losses for different elevation angles. All the antennas will have 0 dB loss in boresight and 3 dB loss when they reach the maximum misalignment angle. The transmitting antenna will have a loss of 1.8 dB and 1.3 dB at $El = 20°$ and $El = 30°$, respectively.

Atmospheric losses

Of the effects causing losses when going through the troposphere mentioned in Section 3.2.1, only electron absorption has a significant impact on the frequency of 400 MHz. In [14] the loss is presented as function of frequency. At 400 MHz, the loss is around 0.2 dB with an elevation angle of 90°. For lower elevation angles, this increases and can be calculated using Equation 3.10. Figure 5.3 shows the absorption which also is the total tropospheric loss, for different elevation angles. For the other two elevation angles of special interest, 20° and 30°, the loss is 0.6 dB and 0.4 dB, respectively.

In the ionosphere, scintillation is the domination loss contributor. Absorption might also contribute to losses, but no data has been found for 400 MHz, and it is assumed to be small and therefore neglected. The bandwidth if 10 kHz is assumed to be too small for dispersion effects. Little data for scintillation for 400 MHz is found, so here, data from another satellite project at NTNU is used. In [25], the ionospheric loss for NUTS is found based on another version of STK and interpolation. This is done for a frequency of 438 MHz and from an Earth station located in Trondheim, Norway (63.42°N, 10.40°E). This

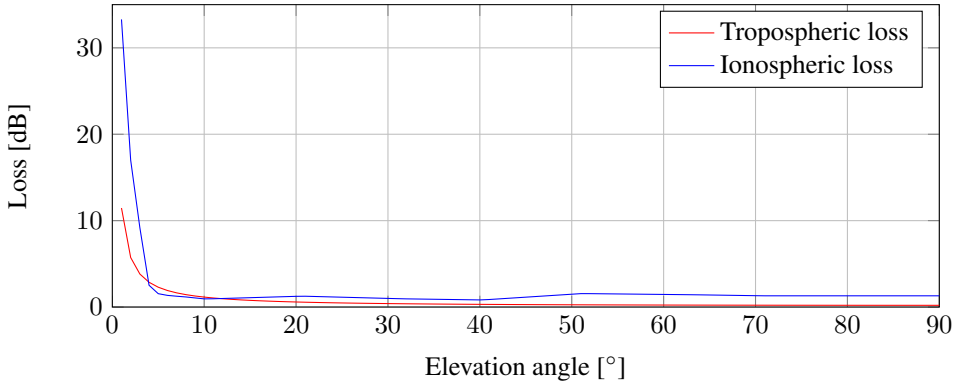

Figure 5.3: Tropospheric and ionospheric losses against the elevation angle. Note that the frequencies are 400 MHz for tropospheric loss and 438 MHz for ionospheric loss.

is south of the area of interest in this thesis, and the frequency is too high. However, these differences are considered reasonable enough, and the data is used, since no other data is available. Figure 5.3 shows the data. The losses vary between 0.8 dB and 1.6 dB for elevations angles between $5°$ and $90°$. For lower elevation angles, the losses increase. For the elevation angles $90°$, $20°$ and $30°$, the loss is 1.3 dB, 1.2 dB and 1.0 dB, respectively.

Passive system loss

Passive system losses are losses between the transmitter and transmitting antenna, and between the receiving antenna and receiver. As mentioned earlier, the system loss in the transmitter is set to zero for now. However, the receiver system loss has to be considered. To calculate this, the system has to be planned. At this time, this has not been done, and the loss is therefore set to 6 dB, which is a little lower than what was operated with in the NUTS project [25].

5.1.3 Link quality

Table 5.2: Received power and signal to noise ratio for the two different receiving antennas and the elevation angles of interest.

$\theta_{B,RX}$ [°]	El [°]	$P_{r,rec}$ [dBm]	C/N [dB]
118.4	90	-124.41	8.14
118.4	20	-136.86	-4.31
104.7	90	-123.17	9.38
104.7	30	-132.47	0.08

The signal power received at the receiver is found using Equation 3.36. In Table 5.2 this is listed for the two antennas at the elevation angles of interest. Since no work has been

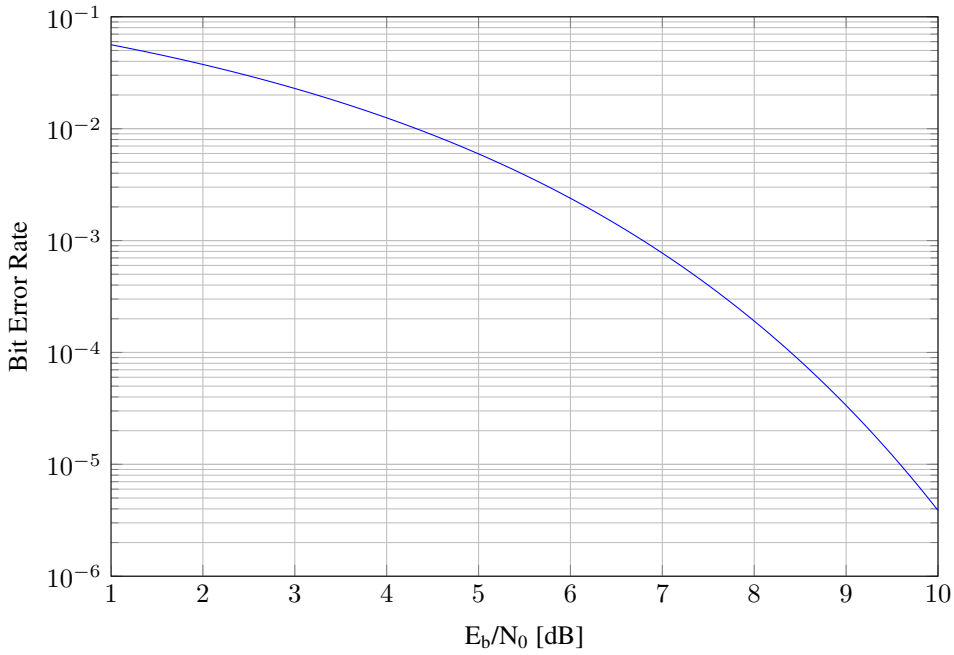

Figure 5.4: BER curve for BPSK.

done on the hardware of the system, only an estimate of the system temperature is possible. Here, a loss factor of 1.5 dB from the antenna to the first low noise amplifier (LNA) in the receiver has been assumed. It is also assumed that the operating temperature in the satellite is around 0°C (273.15 K). The equivalent noise temperature can then be found by Equation 3.40, and it is found to be 112.7 K. The antenna temperature due to the radiation from Earth is 290 K, the Earth's standard temperature. With Equation 3.43 the system temperature is then found to be 402.7 K. With this, and a bandwidth of 10 kHz, the noise power of the receiving system is -132.5 dBmW, from Equation 3.44. The carrier to noise ratio can then be calculated from Equation 3.47, and the results are listed in Table 5.2.

By knowing the carrier to noise ratio, the energy per bit to noise power spectral density ratio can be calculated from Equation 3.50. The final link margin can then be found by comparing this with the required energy per bit to noise power spectral density ratio. This is given in Equation 3.51 and can be found by the BER-curve for BPSK in in Figure 5.4. A bit error rate of 10^{-3}, which gives one error per 1000 bits is assumed to be enough. From the BER-curve, this gives a required energy per bit to noise power spectral density ratio of 6.8 dB.

The final link margin can then be found by Equation 3.53, and is showed for the different receiving antennas and different data rates in Figure 5.5. The complete link budget for the different parameters can also be seen in Table B.1 in Appendix B. It can be seen

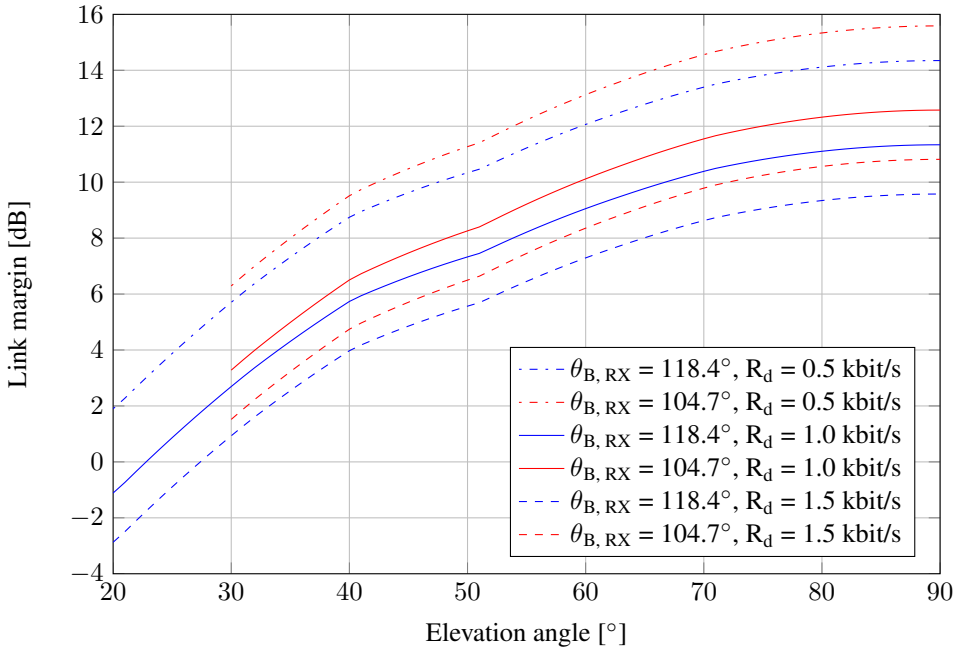

Figure 5.5: Link margin against the elevation angle for the different antennas and data rates.

that the link margin for an elevation angle of 90° is above 9 dB for all combinations of antennas and data rate. At 30° elevation angle they are around 1 dB or higher, while only a data rate of 0.5 kbit/s gives above 0 dB at 20°. For the data rates 1.0 kbit/s and 1.5 kbit/s the link margins cross the zero margin at abound 23° and 27°, respectively.

5.2 Discussion

5.2.1 Antenna specifications and losses

Although a larger beamwidth on the satellite gives more passes with connection and longer connection times, as discussed in Chapter 4, it is penalised with different aspects in the link budget. The gain decreases since it has to radiate over a larger solid angle. As seen here, the gain is 1.2 dBi lower with a beamwidth of 118.4° than for 104.7°. One method of increasing the gain, which has not been discussed in this thesis, is using a steerable antenna. The beamwidth can then be reduced, which also will decrease the pointing loss.

The most significant loss is free space loss. There is not much to do about this, but increasing the elevation angle is beneficial. With a fixed antenna and assuming connection at the elevation angle limits (20° and 30°), there is no difference in the pointing losses. However, both the free space loss and the tropospheric loss increase when lowering the elevation angle, since the propagation path is longer. These differences are 2.3 dB and 0.5

dB, respectively, with advantage to a 30° elevation angle.

The same applies with the basic ionospheric losses, but the increase due to the elevation angle is not significant for elevation angles above about 5°. In Figure 5.3 some variations in the loss can be seen. This can again be seen in Figure 5.5. These variations however, are small compared to the variations that occur with changing conditions in the atmosphere, which can be significant. In the ionosphere, scintillations can give fluctuations as high as 45.8 dB from Equation 3.15, assuming a scintillation index of 1.5. This would cause a complete block in the link margin, and is therefore the most uncertain loss in the link budget. These fluctuations are strongly time varying, and such high values will not last for long. In [20] this time dependence is shown, by showing S_4 at 400 MHz in Kiruna, Sweden. Within about ten minutes the scintillation index goes from $S_4 \approx 0.2$ to $S_4 \approx 1.1$ and down to $S_4 \approx 0.4$. Due to the little data of scintillation strength for 400 MHz, a way to estimate the occurrence of different strengths has not been found. Data does exist for other frequencies, but there is no direct dependence on frequency. The data used in the link budget is therefore just a basis, and does not consider the time varying aspect.

The passive loss in the receiving system has here been set to 6 dB. If we assume the same loss in the transmitting system, a transmitted power of 199 mW is needed to transmit 50 mW. 6 dB loss was what NUTS operated with [25] and has also been operated with here. However, this loss can probably be reduced with 2 - 3 dB by using other components and optimizing the system. The loss between the antenna and the first LNA in the receiver has here been assumed to be 1.5 dB. This is, however, only an assumption and might be smaller or larger. The same can be said about the ambient temperature in the receiver, so the system temperature in the receiver can have some deviations.

5.2.2 Link margin

The required energy per bit to noise power spectral density ratio is a crucial parameter and should be optimized. In this thesis it is found to be 6.8 dB for a bit error rate of 10^{-3} by using uncoded BPSK. Improvements can however be done, by using other modulation schemes and coding. By using QPSK, the data rate can be doubled, compared to using BPSK, since four combinations with two bits can be transmitted instead of two with one bit. This increases the link margin by 3 dB, assuming the same BER-curve as BPSK, witch is achieved by using Grey code, i.e. only one digit differ adjacent values [26]. Uncoded QPSK with the same BER gives an $E_b/N_{0,req}$ of about 7.2 dB, while by using a form of Reed Solomon coding it can be reduced to about 5.9 dB [25].

From Figure 5.5, it can be seen that, as expected, the link margin increases when decreasing data rate. For all antenna scenarios, a data rate of 0.5 kbit/s gives a 3 dB better link budget than 1.0 kbit/s, which again is 1.8 dB better than 1.5 kbit/s. If the same link margin is wanted for the larger data rates as of 0.5 kbit/s, the transmitted power has to be increased to 100 mW and 150 mW for 1.0 kbit/s and 1.5 kbit/s, respectively. For all the different data rates, the link margin is 4.4 dB lower at 20° elevation angle compared to at 30°.

Considering the link margin shown in Figure 5.5, only the elevation angle of 20° and

data rate of 1.0 kbit/s and 1.5 kbit/s goes under the limit of zero dB. However, to ensure communication for most of the time, another margin should be set, so that larger variations in the atmosphere do not block the transmission. An assumed reasonable margin is 5 dB. For that, only transmission using with 0.5 kbit/s is good enough at 30° elevation angle. For the other combinations, a larger transmitted power from the antenna is needed. Table 5.3 shows what power is needed to get a link margin of 5 dB for all of the combinations for their intended elevation angle. From the result of this, 102 mW additional power is needed to compensate for 0.5 kbit/s of extra data rate at 20° elevation angle. For 30° this number is 37 mW.

Table 5.3: Needed power for achieving a link margin of 5 dB for the different combinations at their intended lowest elevation angle.

$\theta_{B,RX}$ [°]	El [°]	R_d [kbit/s]	P_t [mW]
118.4	20	0.5	103
104.7	30	0.5	38
118.4	20	1.0	205
104.7	30	1.0	75
118.4	20	1.5	307
104.7	30	1.5	112

6 Conclusion and future work

Simulations of satellites orbiting in LEO at 600 km height have been performed, with inclinations corresponding to polar orbit and SSO. Coverage for two different Earth station elevation angles, 20° and 30°, have been investigated. When looking at the number of passes with connection during a day, the orbit with the best performance depends on the latitude, and the number generally increases with increasing latitude. In the area with most need for a new communication solution ($\geq 80^\circ$N), the polar orbit shows the best performance. Here, with a 20° elevation angle, connection is established during every satellite revolution, i.e. every 1.5 hours approximately. At 76°N and 72°N, a satellite in SSO has a larger number of passes with connection with seven to eight and four to six passes for 20° and 30° elevation angle, respectively. While the satellite in polar orbit has connection with a minimum of eight nodes during every revolution for both elevation angles, a satellite in SSO has minimum of four with 20° elevation angle and has five consecutive passes in the north without connection to any nodes with 30°. This can be seen in the longest revisit times, where polar orbit has the lowest times at all latitudes. Using SSO, with 30° elevation angle, all nodes have more than half a day as their longest revisit time. In connection times, the advantage of using 20° elevation angle instead of 30° has been found. Both SSO and polar orbit show the same time differences, with the most occurrence of time difference between 100 and 110 seconds.

A link budget for the system has been analysed. Since little is done with specifications, a lot of assumptions have been made. This makes the link budget highly uncertain, however, it gives an prediction of what can be expected. Different antennas with their associated elevations for the Earth station have been compared. The results show that a link is possible for most of the combinations of elevation angle and data rate. Only systems with data rates of 1.0 kbit/s and 1.5 kbit/s show a link margin below 0 dB at an elevation angle of 20°. With a margin of 5 dB, only 0.5 kbit/s and the system with a desired elevation angle 30° is good enough. The cost of transmitted power to use a data rate of 0.5 kbit/s more is 102 mW and 37 mW at elevation angles of 20° and 30°, respectively. The link margin decreases by 4.4 dB at 20° elevation angle, compared to 30°.

Future work

The analysis on the orbits have been done using the free version of STK 10. To get more accurate results and information on coverage and connection, the full version should be used. The minimum required connection time needed for a transmission should be investigated, to find out how many nodes can be operated with.

There is a lot to be done before an accurate link budget can be estimated. The parameters for the transmitting and receiving system are based on other projects and assumptions, while only theoretical antennas have been used. Work on designing these systems should be done. A deeper investigation into the ionospheric losses, regarding the strength and frequency of the scintillation fluctuations, would be beneficial. These can give an indication of the operative time for the system.

Bibliography

[1] The Norwegian Search and Rescue Service. Ministry of Justice and Police. https://www.regjeringen.no/globalassets/upload/kilde/jd/bro/2003/0005/ddd/pdfv/183865-infohefte_engelsk.pdf , accessed Oct 21st, 2014.

[2] S. Marholm, *Antenna Systems for NUTS*. NTNU, Master's Thesis, 2012.

[3] L. Løge, *Arctic Communications System Utilizing Satellites in Highly Elliptical Orbits*. NTNU, Doctoral thesis, 2013.

[4] T. Lewis, *Arctic Connections: Broadband Coming to Top of the World*. LiveScience, 2013. http://www.livescience.com/37205-arctic-broadband-norway-project.html, accessed Aug 19th, 2014.

[5] R. Birkeland, *An Overview of Existing and Future Satellite Systems for Arctic Communication*. The 4S Symposium, 2014.

[6] R. Endresen, *Kjølig til Arktis-nett*. Dagens Næringsliv, Feb 1st, 2014.

[7] B. Narheim, O. Helleren, O. Olsen, R. Olsen, H. Rosshaug, A. Beattie, D. Kekez, and R. Zee, *AISSat-1 Early Results*. 25th Annual AIAA/USU Conference on Small Satellites, 2011.

[8] NASA, *Space Debris and Human Spacecraft*. 2013. http://www.nasa.gov/mission_pages/station/news/orbital_debris.html#.VG50q_mG98kl , accessed Dec 23th, 2014.

[9] J. C. Liou, *An Assessment of the Current LEO Debris Environment and the Need for Active Debris Removal*. NASA. ISTC Space Debris Mitigation Workshop, 2010.

[10] ISO, *Space systems - Estimation of orbit lifetime, ISO 27852*. 2010.

[11] L. Løge. Statsat AS. Information by email. Nov 13th, 2014.

[12] A. J. Bolstad. NTP. Information by email. Oct 14th, 2014.

[13] R. Birkeland, *Overordna spesifikajonar for CAMOS, v. 2*. NTNU, Internal document, 2014.

[14] A. K. Maini and V. Agrawal, *Satellite Technology: Principles and Applications, Second Edition*. John Wiley and Sons Ltd., 2011.

[15] L. J. Ippolito, Jr., *Satellite Communications Systems Engineering: Atmospheric Effects, Satellite Link Design and System Performance*. John Wiley and Sons, Ltd., 2008.

[16] R. J. Boain, *A-B-Cs of Sun-Synchronous Orbit Mission Design*. 14th AAS/AIAA Space Flight Mechanics Conference, 2004.

[17] M. I. Skolnik, *Introduction to Radar Systems, Third edition*. McGraw Hill, 2001.

[18] WeatherOnline Ltd., *Troposphere*. `http://www.weatheronline.co.uk/reports/wxfacts/Troposphere.htm`, accessed Dec 7th, 2014.

[19] INGV, *Ionosphere*. `http://roma2.rm.ingv.it/en/research_areas/4/ionosphere`, accessed Nov 30th, 2014.

[20] ITU, *Ionospheric propagation data and prediction methods required for the design of satellite services and systems, ITU-R P.531-11*. 2012.

[21] P. Misra and P. Enge, *Global Positioning System: Signals, Measurements and Performance, Second Edition*. Ganga-Jamuna Press, 2006.

[22] G. Maral and M. Bousquet, *Satellite Communications Systems: Systems, Techniques and Technology, Fifth edition*. John Wiley & Sons Ltd., 2009.

[23] C. A. Balanis, *Modern Antenna Handbook*. John Wiley and Sons Inc., 2008.

[24] ITU, *Determination of the G/T Ratio for Earth Stations Operating in the Fixed-satellite Service, ITU-R S.733-2*. 2000.

[25] B. L. E. Mendez, *Link Budget for NTNU Test Satellite*. NTNU, Master's Thesis, 2013.

[26] S. Haykin, *Communication Systems, 4th Edition*. John Wiley & Sons Inc., 2001.

Appendix A. Simulation data

A.1 Connection times

Table A.1: Connection times for satellite revolutions for $i = 90^\circ$ and $El = 20^\circ$. Time of simulation is 22 Sep 2014.

Sensor	1	2	3	4	5	6	7	8	9	10	11	12	13	14	15
S11	358,8	358,9	357,3	355,2	354,1	354,9	357,0	358,8	359,0	357,3	354,6	352,7	352,8	354,7	357,3
S12	359,1	357,7	355,6	354,2	354,6	356,5	358,5	359,1	357,8	355,2	353,0	352,6	354,2	356,8	358,8
S13	358,2	356,0	354,4	354,4	356,0	358,1	359,1	358,2	355,8	353,4	352,5	353,7	356,2	358,5	359,1
S14	356,5	354,6	354,2	355,6	357,7	359,1	358,6	356,4	353,8	352,5	353,3	355,6	358,1	359,1	358,2
S21	357,3	356,1	338,9	316,2	304,6	313,6	335,8	354,6	358,2	344,5	321,1	302,8	303,2	321,9	345,2
S22	357,9	343,6	320,8	305,5	310,1	330,7	351,5	359,0	348,7	326,3	305,5	301,2	316,8	340,6	356,9
S23	347,9	325,7	307,3	307,3	325,6	347,8	358,9	352,3	331,6	309,1	300,3	312,2	335,5	354,6	358,2
S24	330,8	310,1	305,4	320,7	343,5	357,9	355,2	336,8	313,3	300,5	308,1	330,3	351,5	359,0	348,8
S31	354,3	350,3	297,6	213,9	157,1	202,6	287,4	345,8	356,7	318,3	242,7	166,4	168,1	245,4	320,2
S32	355,5	312,7	232,8	161,9	185,8	269,9	336,8	358,7	330,4	261,0	179,5	158,4	226,8	306,4	353,2
S33	325,9	251,8	172,0	171,7	251,4	325,6	358,3	340,6	278,6	195,4	153,5	208,5	291,1	346,8	356,3
S34	270,3	186,1	161,8	232,4	312,4	355,4	348,6	295,0	213,0	154,2	191,2	274,3	338,3	358,6	328,6
S41	349,6	341,7	221,8	0,0	0,0	0,0	192,8	332,7	354,4	274,6	0,0	0,0	0,0	0,0	278,8
S42	352,0	259,9	0,0	0,0	0,0	132,4	314,0	358,3	301,1	105,1	0,0	0,0	0,0	247,1	347,4
S43	290,3	0,0	0,0	0,0	0,0	289,8	357,4	322,2	171,7	0,0	0,0	0,0	208,0	334,9	353,7
S44	133,9	0,0	0,0	0,0	259,2	351,8	338,4	218,6	0,0	0,0	0,0	157,7	317,5	358,1	296,4
S51	343,1	330,5	0,0	0,0	0,0	0,0	0,0	315,2	351,1	202,5	0,0	0,0	0,0	0,0	211,8
S52	347,7	167,1	0,0	0,0	0,0	0,0	282,0	357,6	256,9	0,0	0,0	0,0	0,0	132,4	339,4
S53	236,2	0,0	0,0	0,0	0,0	235,2	356,4	295,9	0,0	0,0	0,0	0,0	0,0	318,0	350,4
S54	0,0	0,0	0,0	0,0	165,3	347,4	324,1	0,0	0,0	0,0	0,0	0,0	287,3	357,5	248,4

Table A.2: Connection times for satellite revolutions for $i = 98°$ and $El = 20°$. Time of simulation is 22 Sep 2014.

Sensor	1	2	3	4	5	6	7	8	9	10	11	12	13	14	15
S11	259,2	230,4	198,1	170,3	158,2	168,7	195,8	228,1	257,3	279,9	294,6	301,6	301,4	294,0	278,9
S12	237,0	205,0	175,3	158,9	164,7	189,2	221,2	251,5	275,7	292,1	300,7	302,1	296,2	282,8	261,5
S13	212,0	181,0	160,7	161,5	182,9	214,2	245,4	271,1	289,2	299,5	302,4	298,1	286,4	266,8	239,8
S14	187,2	163,6	159,4	177,1	207,2	239,1	266,2	286,0	297,9	302,4	299,6	289,5	271,6	246,1	215,0
S21	276,5	181,0	0,0	0,0	0,0	0,0	0,0	170,6	271,5	321,2	343,1	350,2	350,1	342,4	319,5
S22	207,8	0,0	0,0	0,0	0,0	0,0	134,9	255,5	313,4	340,0	349,5	350,6	345,0	326,3	282,3
S23	60,1	0,0	0,0	0,0	0,0	84,3	236,9	304,2	336,2	348,3	350,8	347,0	332,0	294,7	217,8
S24	0,0	0,0	0,0	0,0	0,0	215,3	293,4	331,4	346,8	350,8	348,5	336,6	305,3	239,1	91,3
S31	292,8	107,7	0,0	0,0	0,0	0,0	0,0	69,3	285,7	345,2	355,3	349,8	350,1	355,4	343,7
S32	175,1	0,0	0,0	0,0	0,0	0,0	0,0	261,5	338,0	355,4	351,0	349,2	354,7	349,2	300,8
S33	0,0	0,0	0,0	0,0	0,0	0,0	230,7	328,2	354,6	352,3	348,7	353,6	352,7	316,9	195,5
S34	0,0	0,0	0,0	0,0	0,0	190,5	315,3	352,4	353,7	348,8	352,2	354,7	329,4	234,5	0,0
S41	307,7	0,0	0,0	0,0	0,0	0,0	0,0	0,0	299,4	354,8	335,6	301,7	302,9	337,4	354,3
S42	137,8	0,0	0,0	0,0	0,0	0,0	0,0	269,1	351,5	342,9	307,3	298,6	329,5	355,0	316,8
S43	0,0	0,0	0,0	0,0	0,0	0,0	227,3	344,2	349,0	314,3	296,5	321,3	352,9	333,7	173,6
S44	0,0	0,0	0,0	0,0	0,0	165,3	332,2	353,3	322,2	296,6	313,5	348,4	345,2	232,6	0,0
S51	320,9	0,0	0,0	0,0	0,0	0,0	0,0	0,0	312,1	350,8	277,6	169,8	174,2	282,9	352,2
S52	92,6	0,0	0,0	0,0	0,0	0,0	0,0	278,0	354,6	299,2	190,1	157,9	259,7	344,5	330,1
S53	0,0	0,0	0,0	0,0	0,0	0,0	226,7	352,8	318,2	213,4	149,2	235,3	332,4	345,5	153,1
S54	0,0	0,0	0,0	0,0	0,0	140,3	344,2	333,9	238,0	149,7	210,8	316,3	353,3	233,5	0,0

Table A.3: Connection times for satellite revolutions for $i = 90^\circ$ and $El = 30^\circ$. Time of simulation is 22 Sep 2014.

Sensor	1	2	3	4	5	6	7	8	9	10	11	12	13	14	15
S11	255,2	255,1	252,5	249,3	247,7	249,0	252,0	254,8	255,3	253,1	249,6	246,9	247,0	249,7	253,2
S12	255,3	253,2	249,9	247,9	248,5	251,3	254,4	255,5	253,8	250,4	247,3	246,7	248,9	252,5	255,1
S13	253,8	250,6	248,1	248,1	250,6	253,8	255,5	254,4	251,2	247,8	246,6	248,3	251,8	254,7	255,4
S14	251,3	248,5	247,9	249,9	253,2	255,3	254,8	251,9	248,4	246,6	247,7	251,0	254,2	255,5	254,0
S21	253,3	250,8	224,6	187,8	167,0	183,3	219,8	248,5	254,4	235,4	199,9	169,2	169,8	201,1	236,3
S22	253,5	231,9	195,5	168,6	177,0	211,8	243,9	255,4	241,4	208,2	174,0	166,3	193,0	229,6	252,7
S23	238,4	203,7	172,0	171,9	203,5	238,3	255,0	246,4	216,3	180,1	164,7	185,4	222,2	249,6	254,0
S24	211,9	177,1	168,5	195,4	231,8	253,5	250,4	224,1	187,2	164,9	178,5	214,3	245,3	255,2	239,8
S31	249,3	242,2	153,9	0,0	0,0	0,0	132,6	235,5	252,6	195,5	0,0	0,0	0,0	0,0	198,6
S32	250,0	181,8	0,0	0,0	0,0	87,5	221,6	255,1	214,6	71,9	0,0	0,0	0,0	175,7	247,7
S33	204,2	0,0	0,0	0,0	0,0	203,8	254,2	229,8	121,0	0,0	0,0	0,0	147,4	238,8	251,3
S34	88,6	0,0	0,0	0,0	181,3	249,9	241,4	155,0	0,0	0,0	0,0	110,8	226,4	254,8	208,6
S41	243,0	229,4	0,0	0,0	0,0	0,0	0,0	215,4	249,6	111,8	0,0	0,0	0,0	0,0	121,9
S42	245,0	48,7	0,0	0,0	0,0	0,0	184,5	254,7	166,5	0,0	0,0	0,0	0,0	0,0	239,8
S43	139,4	0,0	0,0	0,0	0,0	138,2	253,2	202,1	0,0	0,0	0,0	0,0	0,0	221,5	247,6
S44	0,0	0,0	0,0	0,0	45,0	244,8	226,8	0,0	0,0	0,0	0,0	0,0	194,4	254,2	151,8
S51	233,9	212,4	0,0	0,0	0,0	0,0	0,0	187,0	245,3	0,0	0,0	0,0	0,0	0,0	0,0
S52	238,9	0,0	0,0	0,0	0,0	0,0	121,5	254,2	56,9	0,0	0,0	0,0	0,0	0,0	228,5
S53	0,0	0,0	0,0	0,0	0,0	0,0	252,0	157,4	0,0	0,0	0,0	0,0	0,0	195,6	243,0
S54	0,0	0,0	0,0	0,0	0,0	238,5	205,4	0,0	0,0	0,0	0,0	0,0	140,6	253,6	0,0

Table A.4: Connection times for satellite revolutions for $i = 98°$ and $El = 30°$. Time of simulation is 22 Sep 2014.

Sensor	1	2	3	4	5	6	7	8	9	10	11	12	13	14	15
S11	56,4	0,0	0,0	0,0	0,0	0,0	0,0	0,0	46,7	120,4	151,9	165,4	165,1	150,8	118,1
S12	0,0	0,0	0,0	0,0	0,0	0,0	0,0	0,0	110,1	146,9	163,8	166,3	155,2	127,2	66,4
S13	0,0	0,0	0,0	0,0	0,0	0,0	0,0	98,0	141,1	161,4	166,9	158,8	135,0	84,9	0,0
S14	0,0	0,0	0,0	0,0	0,0	0,0	83,1	134,2	158,5	166,8	161,7	141,8	99,4	0,0	0,0
S21	112,3	0,0	0,0	0,0	0,0	0,0	0,0	0,0	99,3	199,7	234,0	244,7	244,5	233,0	196,8
S22	0,0	0,0	0,0	0,0	0,0	0,0	0,0	35,5	186,6	229,4	243,5	245,2	236,9	207,9	126,2
S23	0,0	0,0	0,0	0,0	0,0	0,0	0,0	170,3	223,5	241,9	245,6	239,9	216,9	152,3	0,0
S24	0,0	0,0	0,0	0,0	0,0	0,0	149,8	216,0	239,6	245,6	242,1	224,2	172,3	0,0	0,0
S31	148,8	0,0	0,0	0,0	0,0	0,0	0,0	0,0	134,1	237,3	252,7	245,3	245,7	252,8	235,1
S32	0,0	0,0	0,0	0,0	0,0	0,0	0,0	67,1	226,4	252,7	246,9	244,4	251,9	243,3	164,3
S33	0,0	0,0	0,0	0,0	0,0	0,0	0,0	211,1	251,4	248,8	243,8	250,4	248,6	192,6	0,0
S34	0,0	0,0	0,0	0,0	0,0	0,0	190,0	248,2	250,6	243,8	248,6	251,6	213,0	0,0	0,0
S41	177,2	0,0	0,0	0,0	0,0	0,0	0,0	0,0	162,0	251,9	225,0	170,8	172,8	227,7	251,2
S42	0,0	0,0	0,0	0,0	0,0	0,0	0,0	93,6	246,9	235,7	180,5	165,3	215,9	252,5	192,8
S43	0,0	0,0	0,0	0,0	0,0	0,0	0,0	236,0	244,3	192,1	161,5	203,3	249,7	220,1	0,0
S44	0,0	0,0	0,0	0,0	0,0	0,0	217,7	250,2	204,7	161,7	190,8	243,5	237,5	0,0	0,0
S51	200,0	0,0	0,0	0,0	0,0	0,0	0,0	0,0	185,3	247,1	123,8	0,0	0,0	135,4	249,0
S52	0,0	0,0	0,0	0,0	0,0	0,0	0,0	117,7	252,2	166,7	0,0	0,0	75,9	238,3	214,8
S53	0,0	0,0	0,0	0,0	0,0	0,0	0,0	249,2	198,7	0,0	0,0	0,0	220,5	238,4	0,0
S54	0,0	0,0	0,0	0,0	0,0	0,0	236,5	222,8	0,0	0,0	0,0	195,6	249,9	0,0	0,0

Table A.5: Connection times for satellite revolutions for $i = 90^\circ$ and $El = 20^\circ$. Time of simulation is 23 Sep 2014.

Sensor	1	2	3	4	5	6	7	8	9	10	11	12	13	14	15
S11	359,0	358,8	356,9	354,9	354,1	355,2	357,4	359,0	358,8	356,8	354,2	352,6	353,0	355,1	357,7
S12	359,0	357,4	355,3	354,1	354,9	356,9	358,7	359,0	357,4	354,8	352,8	352,7	354,6	357,2	359,0
S13	357,8	355,7	354,2	354,6	356,4	358,4	359,1	357,9	355,3	353,1	352,5	354,1	356,7	358,7	359,0
S14	356,1	354,4	354,3	355,9	358,1	359,1	358,3	355,9	353,5	352,5	353,6	356,1	358,4	359,1	357,9
S21	358,4	354,2	335,0	313,1	304,7	316,9	339,6	356,4	357,0	341,0	317,2	301,4	305,3	325,9	348,4
S22	356,6	340,0	317,2	304,7	312,8	334,6	353,9	358,5	345,5	322,3	303,4	302,6	320,7	344,2	358,1
S23	344,6	321,9	305,8	309,3	329,5	350,7	359,0	349,6	327,6	306,3	300,9	315,7	339,4	356,4	357,0
S24	326,9	307,9	306,8	324,4	346,8	358,7	353,1	332,8	310,0	300,3	311,2	334,4	353,9	358,5	345,6
S31	357,2	344,6	284,9	200,0	157,5	216,7	299,9	351,2	353,6	307,6	228,4	159,0	178,3	259,5	329,5
S32	351,7	301,2	218,2	157,7	198,5	283,5	343,9	357,4	321,2	246,9	169,1	165,5	241,1	317,2	356,5
S33	315,9	237,2	163,8	182,3	265,8	334,4	358,8	333,0	265,1	182,9	156,8	222,6	303,1	351,9	352,9
S34	256,1	174,9	169,0	247,1	322,8	357,8	342,6	282,5	199,3	153,2	204,4	287,3	345,1	357,1	319,0
S41	355,3	330,3	185,3	0,0	0,0	0,0	227,9	343,5	348,2	250,0	0,0	0,0	0,0	97,7	299,1
S42	344,5	231,3	0,0	0,0	0,0	180,9	328,9	355,7	281,2	0,0	0,0	0,0	0,0	272,1	353,9
S43	267,5	0,0	0,0	0,0	114,1	309,0	358,5	306,4	123,5	0,0	0,0	0,0	238,9	345,0	347,0
S44	52,9	0,0	0,0	0,0	283,4	356,6	326,4	183,6	0,0	0,0	0,0	197,7	331,3	355,1	274,7
S51	352,6	311,0	0,0	0,0	0,0	0,0	41,9	333,6	340,8	140,9	0,0	0,0	0,0	0,0	253,1
S52	335,2	66,1	0,0	0,0	0,0	0,0	308,6	353,3	216,8	0,0	0,0	0,0	0,0	197,0	350,2
S53	186,0	0,0	0,0	0,0	0,0	272,7	358,0	267,0	0,0	0,0	0,0	0,0	104,7	335,3	339,5
S54	0,0	0,0	0,0	0,0	221,8	355,1	303,3	0,0	0,0	0,0	0,0	0,0	311,9	352,7	202,8

Table A.6: Connection times for satellite revolutions for $i = 98°$ and $El = 20°$. Time of simulation is 23 Sep 2014.

Sensor	1	2	3	4	5	6	7	8	9	10	11	12	13	14	15
S11	256,0	226,4	194,2	167,7	158,2	171,4	199,8	232,0	260,5	282,1	295,8	302,0	300,9	292,6	276,5
S12	233,2	201,0	172,3	158,3	166,9	193,0	225,2	254,9	278,1	293,5	301,3	301,7	295,0	280,6	258,4
S13	208,0	177,7	159,5	163,2	186,5	218,2	249,0	273,8	290,9	300,2	302,2	297,1	284,4	263,8	236,0
S14	183,6	161,8	160,5	180,4	211,3	242,8	269,1	287,9	298,9	302,4	298,8	287,7	268,9	242,5	210,9
S21	267,9	163,0	0,0	0,0	0,0	0,0	0,0	187,8	279,8	325,1	344,6	350,5	349,6	340,7	315,0
S22	192,9	0,0	0,0	0,0	0,0	0,0	156,6	265,0	318,1	341,9	349,9	350,3	343,6	322,5	274,3
S23	0,0	0,0	0,0	0,0	0,0	116,3	248,0	309,7	338,5	349,0	350,7	345,9	328,8	287,8	204,0
S24	0,0	0,0	0,0	0,0	49,0	228,2	299,9	334,3	347,7	350,9	347,7	334,1	299,4	227,2	43,6
S31	280,5	0,0	0,0	0,0	0,0	0,0	0,0	127,5	297,4	348,3	354,9	349,3	350,8	355,5	339,5
S32	140,9	0,0	0,0	0,0	0,0	0,0	0,0	276,1	342,4	355,4	350,3	349,7	355,2	346,3	289,6
S33	0,0	0,0	0,0	0,0	0,0	0,0	249,4	334,2	355,2	351,5	348,9	354,3	350,9	308,1	166,8
S34	0,0	0,0	0,0	0,0	0,0	215,1	323,1	353,9	352,9	348,7	353,0	353,8	322,5	213,4	0,0
S41	293,1	0,0	0,0	0,0	0,0	0,0	0,0	0,0	312,9	355,1	331,0	299,3	306,1	341,6	352,3
S42	52,9	0,0	0,0	0,0	0,0	0,0	0,0	287,7	353,8	338,8	303,9	300,9	334,1	355,0	304,0
S43	0,0	0,0	0,0	0,0	0,0	0,0	253,1	348,9	345,7	310,1	297,5	326,0	354,5	324,7	121,5
S44	0,0	0,0	0,0	0,0	0,0	204,4	339,7	351,1	317,6	296,3	317,9	351,3	339,2	201,7	0,0
S51	305,2	0,0	0,0	0,0	0,0	0,0	0,0	0,0	326,3	346,3	264,2	160,5	186,0	295,4	354,3
S52	0,0	0,0	0,0	0,0	0,0	0,0	0,0	299,3	353,1	287,0	177,8	166,6	273,3	349,5	317,1
S53	0,0	0,0	0,0	0,0	0,0	0,0	259,0	354,6	307,6	199,7	153,2	249,5	339,9	337,7	53,7
S54	0,0	0,0	0,0	0,0	0,0	196,7	350,0	325,3	223,8	148,2	224,9	326,0	349,7	193,1	0,0

Table A.7: Connection times for satellite revolutions for $i = 90^\circ$ and $El = 30^\circ$. Time of simulation is 23 Sep 2014.

Sensor	1	2	3	4	5	6	7	8	9	10	11	12	13	14	15
S11	255,4	254,8	251,9	248,9	247,8	249,4	252,6	255,1	255,1	252,6	249,0	246,7	247,3	250,3	253,8
S12	255,1	252,7	249,4	247,8	248,8	251,9	254,7	255,4	253,3	249,8	247,0	246,9	249,5	253,1	255,3
S13	253,3	250,1	247,9	248,4	251,2	254,2	255,5	253,9	250,5	247,4	246,7	248,8	252,4	255,0	255,2
S14	250,8	248,2	248,0	250,4	253,7	255,4	254,5	251,3	248,0	246,6	248,1	251,6	254,6	255,4	253,5
S21	254,7	247,9	218,7	182,3	167,1	188,9	225,8	251,3	252,9	230,2	193,7	166,6	173,5	207,5	240,9
S22	251,5	226,4	189,5	167,2	181,8	218,0	247,5	254,8	236,8	201,8	170,1	168,8	199,3	234,9	254,3
S23	233,5	197,4	169,2	175,7	209,9	242,7	255,4	242,6	210,1	175,3	165,8	191,2	228,0	252,1	252,2
S24	205,6	173,0	171,0	201,6	236,9	254,8	247,5	218,1	181,6	164,6	183,7	220,4	248,7	254,4	235,0
S31	253,2	233,7	127,0	0,0	0,0	0,0	158,4	243,6	248,3	177,8	0,0	0,0	0,0	66,3	213,2
S32	244,3	160,9	0,0	0,0	0,0	123,8	232,6	253,5	200,3	0,0	0,0	0,0	0,0	193,8	252,2
S33	187,4	0,0	0,0	0,0	73,4	217,9	255,2	218,5	85,6	0,0	0,0	0,0	169,8	246,0	246,2
S34	16,1	0,0	0,0	0,0	199,1	253,6	232,8	129,6	0,0	0,0	0,0	139,9	236,3	252,4	192,7
S41	250,8	211,6	0,0	0,0	0,0	0,0	0,0	232,2	241,0	0,0	0,0	0,0	0,0	0,0	162,9
S42	233,7	0,0	0,0	0,0	0,0	0,0	209,3	251,4	127,1	0,0	0,0	0,0	0,0	105,7	248,9
S43	80,3	0,0	0,0	0,0	0,0	175,6	255,0	175,9	0,0	0,0	0,0	0,0	0,0	236,3	237,5
S44	0,0	0,0	0,0	0,0	123,9	251,9	208,6	0,0	0,0	0,0	0,0	0,0	216,2	249,7	102,1
S51	247,3	179,7	0,0	0,0	0,0	0,0	0,0	217,2	230,6	0,0	0,0	0,0	0,0	0,0	35,9
S52	219,8	0,0	0,0	0,0	0,0	0,0	175,4	248,3	0,0	0,0	0,0	0,0	0,0	0,0	244,1
S53	0,0	0,0	0,0	0,0	0,0	97,3	254,6	92,2	0,0	0,0	0,0	0,0	0,0	222,4	226,4
S54	0,0	0,0	0,0	0,0	0,0	250,0	170,7	0,0	0,0	0,0	0,0	0,0	185,5	246,5	0,0

Table A.8: Connection times for satellite revolutions for $i = 98°$ and $El = 30°$. Time of simulation is 23 Sep 2014.

Sensor	1	2	3	4	5	6	7	8	9	10	11	12	13	14	15
S11	38,5	0,0	0,0	0,0	0,0	0,0	0,0	0,0	62,2	125,6	154,4	166,1	164,1	147,9	112,2
S12	0,0	0,0	0,0	0,0	0,0	0,0	0,0	30,4	116,2	149,9	164,8	165,7	152,8	122,1	52,3
S13	0,0	0,0	0,0	0,0	0,0	0,0	0,0	105,2	144,6	162,9	166,6	156,8	130,7	74,9	0,0
S14	0,0	0,0	0,0	0,0	0,0	0,0	92,1	138,3	160,3	166,9	160,1	138,0	91,4	0,0	0,0
S21	88,8	0,0	0,0	0,0	0,0	0,0	0,0	0,0	120,4	206,1	236,3	245,1	243,8	230,3	189,2
S22	0,0	0,0	0,0	0,0	0,0	0,0	0,0	79,5	194,5	232,2	244,3	244,8	234,8	201,8	106,7
S23	0,0	0,0	0,0	0,0	0,0	0,0	0,0	180,2	227,0	242,9	245,4	238,3	212,0	138,2	0,0
S24	0,0	0,0	0,0	0,0	0,0	0,0	162,3	220,5	241,0	245,6	240,9	220,2	161,4	0,0	0,0
S31	122,3	0,0	0,0	0,0	0,0	0,0	0,0	0,0	157,8	242,0	252,2	244,6	246,6	252,8	228,7
S32	0,0	0,0	0,0	0,0	0,0	0,0	0,0	111,9	233,2	252,8	245,9	245,1	252,5	239,0	142,4
S33	0,0	0,0	0,0	0,0	0,0	0,0	0,0	220,5	252,4	247,7	244,1	251,4	245,9	177,5	0,0
S34	0,0	0,0	0,0	0,0	0,0	0,0	203,0	250,3	249,6	243,7	249,6	250,1	202,0	0,0	0,0
S41	149,8	0,0	0,0	0,0	0,0	0,0	0,0	0,0	186,3	252,6	218,2	166,5	178,5	233,9	248,3
S42	0,0	0,0	0,0	0,0	0,0	0,0	0,0	138,9	250,5	229,8	174,6	169,3	222,9	252,3	170,6
S43	0,0	0,0	0,0	0,0	0,0	0,0	16,2	243,1	239,7	185,2	163,2	210,6	251,8	205,8	0,0
S44	0,0	0,0	0,0	0,0	0,0	0,0	229,3	247,2	197,4	161,0	197,9	247,5	228,5	0,0	0,0
S51	173,2	0,0	0,0	0,0	0,0	0,0	0,0	0,0	208,7	240,8	89,8	0,0	0,0	159,8	251,8
S52	0,0	0,0	0,0	0,0	0,0	0,0	0,0	162,4	250,2	143,7	0,0	0,0	114,0	245,3	193,7
S53	0,0	0,0	0,0	0,0	0,0	0,0	58,8	252,0	181,3	0,0	0,0	23,4	231,6	226,5	0,0
S54	0,0	0,0	0,0	0,0	0,0	0,0	245,1	209,8	0,0	0,0	0,0	210,9	244,5	0,0	0,0

A.2 Revisit times

Table A.9: Minimum and maximum revisit time (in hours) for $El = 20^{\circ}$.

	90° inclination		98° inclination	
Sensor	**Minimum**	**Maximum**	**Minimum**	**Maximum**
S11	1,51	1,52	1,53	1,57
S12	1,51	1,52	1,53	1,57
S13	1,51	1,52	1,53	1,57
S14	1,51	1,52	1,53	1,57
S21	1,51	1,54	1,50	9,69
S22	1,51	1,54	1,50	9,69
S23	1,51	1,54	1,51	9,69
S24	1,51	1,54	1,51	8,17
S31	1,51	1,58	1,50	11,33
S32	1,51	1,58	1,50	11,33
S33	1,51	1,59	1,50	11,38
S34	1,51	1,59	1,50	11,32
S41	1,52	6,49	1,50	12,95
S42	1,52	7,88	1,50	11,37
S43	1,52	6,50	1,50	11,36
S44	1,52	6,50	1,50	11,36
S51	1,52	8,16	1,50	12,98
S52	1,52	8,16	1,50	12,98
S53	1,52	8,15	1,50	11,40
S54	1,52	9,44	1,50	11,40

Table A.10: Minimum and maximum revisit time (in hours) for $El = 30^{\circ}$.

	90° inclination		98° inclination	
Sensor	**Minimum**	**Maximum**	**Minimum**	**Maximum**
S11	1,54	1,55	1,56	12,91
S12	1,54	1,55	1,56	12,91
S13	1,54	1,55	1,56	14,51
S14	1,54	1,55	1,56	14,51
S21	1,54	1,58	1,53	12,93
S22	1,54	1,58	1,53	12,93
S23	1,54	1,58	1,53	14,53
S24	1,54	1,58	1,53	14,53
S31	1,55	6,48	1,53	12,96
S32	1,55	7,94	1,53	12,96
S33	1,54	6,49	1,53	14,55
S34	1,54	6,49	1,53	14,55
S41	1,55	9,74	1,53	12,99
S42	1,55	9,74	1,53	12,99
S43	1,55	9,51	1,53	13,00
S44	1,55	9,50	1,53	14,58
S51	1,55	9,78	1,53	13,02
S52	1,56	11,07	1,54	13,02
S53	1,55	9,49	1,53	13,03
S54	1,55	11,39	1,53	14,60

A.3 Time differences between 20°and 30°elevation angle

Table A.11: Time difference between $El = 20°$ and $El = 30°$ for $i = 90$. Numbers in *cursive* means that only $El = 20°$ have connection. Time of simulation is 23 Sep 2014.

Sensor	**1**	**2**	**3**	**4**	**5**	**6**	**7**	**8**	**9**	**10**	**11**	**12**	**13**	**14**	**15**
S11	103,6	104,0	105,0	106,0	106,4	105,8	104,8	103,9	103,7	104,3	105,2	105,8	105,7	104,9	104,0
S12	103,8	104,7	105,8	106,4	106,0	105,0	104,0	103,6	104,1	105,0	105,8	105,8	105,1	104,1	103,6
S13	104,5	105,6	106,3	106,2	105,2	104,2	103,6	103,9	104,8	105,7	105,9	105,3	104,3	103,7	103,8
S14	105,4	106,2	106,3	105,5	104,4	103,7	103,8	104,6	105,5	105,9	105,5	104,5	103,8	103,7	104,5
S21	103,7	106,3	116,4	130,8	137,6	128,0	113,8	105,2	104,1	110,8	123,5	134,8	131,8	118,4	107,5
S22	105,1	113,6	127,7	137,5	131,0	116,6	106,4	103,7	108,7	120,5	133,2	133,8	121,4	109,3	103,8
S23	111,1	124,5	136,6	133,7	119,6	108,0	103,6	107,0	117,5	131,0	135,1	124,5	111,5	104,3	104,8
S24	121,3	134,8	135,8	122,8	110,0	103,9	105,6	114,7	128,3	135,7	127,5	113,9	105,3	104,1	110,6
S31	104,0	111,0	157,9	*200,0*	*157,5*	*216,7*	141,5	107,6	105,3	129,8	*228,4*	*159,0*	*178,3*	193,2	116,3
S32	107,4	140,3	*218,2*	*157,7*	*198,5*	159,7	111,3	103,9	120,9	*246,9*	*169,1*	*165,5*	*241,1*	123,4	104,2
S33	128,5	*237,2*	*163,8*	*182,3*	192,3	116,5	103,6	114,5	179,5	*182,9*	*156,8*	*222,6*	133,3	105,9	106,7
S34	240,0	*174,9*	*169,0*	*247,1*	123,7	104,3	109,8	152,8	*199,3*	*153,2*	*204,4*	147,4	108,8	104,7	126,3
S41	104,5	118,7	*185,3*				*227,9*	111,3	107,2	*250,0*				*97,7*	136,2
S42	110,8	*231,3*				*180,9*	119,5	104,3	154,0					166,4	105,0
S43	187,2				*114,1*	133,4	103,5	130,5	*123,5*				*238,9*	108,6	109,5
S44	*52,9*				159,4	104,7	117,8	*183,6*				*197,7*	115,1	105,4	172,6
S51	105,2	131,3					*41,9*	116,4	110,2	*140,9*					217,2
S52	115,4	*66,1*					133,2	104,9	*216,8*					*197,0*	106,2
S53	*186,0*					175,3	103,4	174,8					*104,7*	112,9	113,1
S54					*221,8*	105,1	132,5						126,3	106,3	*202,8*

Table A.12: Time difference between $El = 20°$ and $El = 30°$ for $i = 98$. Numbers in *cursive* means that only $El = 20°$ have connection. Time of simulation is 23 Sep 2014.

Sensor	1	2	3	4	5	6	7	8	9	10	11	12	13	14	15
S11	217,5	*226,4*	*194,2*	*167,7*	*158,2*	*171,4*	*199,8*	*232,0*	198,3	156,5	141,4	135,9	136,8	144,6	164,3
S12	*233,2*	*201,0*	*172,3*	*158,3*	*166,9*	*193,0*	*225,2*	224,5	161,9	143,6	136,5	136,1	142,2	158,5	206,1
S13	*208,0*	*177,7*	*159,5*	*163,2*	*186,5*	*218,2*	*249,0*	168,6	146,3	137,4	135,6	140,2	153,7	188,9	*236,0*
S14	*183,6*	*161,8*	*160,5*	*180,4*	*211,3*	*242,8*	177,0	149,6	138,6	135,5	138,7	149,7	177,5	*242,5*	*210,9*
S21	179,1	*163,0*						*187,8*	159,4	119,1	108,3	105,4	105,8	110,3	125,7
S22	*192,9*						*156,6*	185,6	123,6	109,7	105,7	105,5	108,8	120,7	167,6
S23						*116,3*	*248,0*	129,5	111,5	106,1	105,3	107,7	116,9	149,6	*204,0*
S24					*49,0*	*228,2*	137,6	113,8	106,8	105,2	106,8	113,9	138,0	*227,2*	*43,6*
S31	158,1							*127,5*	139,6	106,3	102,7	104,7	104,2	102,7	110,8
S32	*140,9*							164,3	109,3	102,6	104,3	104,6	102,6	107,3	147,2
S33							*249,4*	113,6	102,9	103,9	104,9	102,9	105,0	130,6	*166,8*
S34						*215,1*	120,1	103,6	103,4	105,0	103,3	103,6	120,5	*213,4*	
S41	143,3								126,6	102,5	112,8	132,8	127,7	107,8	104,1
S42	*52,9*							148,8	103,4	109,0	129,3	131,6	111,3	102,7	133,4
S43							236,9	105,8	106,0	124,9	134,3	115,4	102,7	118,9	*121,5*
S44						*204,4*	110,4	103,9	120,2	135,2	120,0	103,8	110,7	*201,7*	
S51	132,0								117,6	105,5	174,3	*160,5*	*186,0*	135,6	102,5
S52								136,9	102,9	143,3	*177,8*	*166,6*	159,3	104,2	123,4
S53							200,1	102,6	126,3	*199,7*	*153,2*	226,2	108,3	111,2	*53,7*
S54						*196,7*	104,9	115,5	*223,8*	*148,2*	*224,9*	115,1	105,1	*193,1*	

Appendix B. Link budget

Table B.1: Link budget.

Parameter	Unit	$\theta_B = 118.4°$		$\theta_B = 104.7°$	
f	[MHz]	400	400	400	400
h	[km]	600	600	600	600
El	[°]	90	20	90	30
d	[km]	600.0	1392.4	600.0	1075.2
P_t	[mW]	50	50	50	50
P_t	[dBmW]	16.99	16.99	16.99	16.99
L_{TX}	[dB]	0	0	0	0
G_t	[dBi]	3	3	3	3
EIRP	[dBmW]	19.99	19.99	19.99	19.99
FSL	[dB]	140.05	147.36	140.05	145.12
PLF	[dB]	3	3	3	3
$L_{pt,TX}$	[dB]	0	1.81	0	1.33
$L_{pt,RX}$	[dB]	0	3	0	3
L_{trop}	[dB]	0.20	0.58	0.20	0.40
L_{ion}	[dB]	1.30	1.24	1.30	1.00
G_r	[dBi]	6.15	6.15	7.39	7.39
$P_{r,ant}$	[dBmW]	-118.41	-130.86	-117.17	-126.47
L_{RX}	[dB]	6	6	6	6
$P_{r,rec}$	[dBmW]	-124.41	-136.86	-123.17	-132.47
T_{RX}	[K]	402.7	402.7	402.7	402.7
B	[kHz]	10	10	10	10
N	[dBmW]	-132.55	-132.55	-132.55	-132.55
C/N	[dB]	8.14	-4.31	9.38	0.08
R_d	[kbit/s]	0.5	0.5	0.5	0.5
E_b/N_0	[dB]	21.15	8.70	22.39	13.09
$E_b/N_{0,req}$	[dB]	6.80	6.80	6.80	6.80
LM	**[dB]**	**14.35**	**1.90**	**15.59**	**6.29**
R_d	[kbit/s]	1.0	1.0	1.0	1.0
E_b/N_0	[dB]	18.14	5.69	19.38	10.08
$E_b/N_{0,req}$	[dB]	6.80	6.80	6.80	6.80
LM	**[dB]**	**11.34**	**-1.11**	**12.58**	**3.28**
R_d	[kbit/s]	1.5	1.5	1.5	1.5
E_b/N_0	[dB]	16.38	3.93	17.62	8.32
$E_b/N_{0,req}$	[dB]	6.80	6.80	6.80	6.80
LM	**[dB]**	**9.58**	**-2.87**	**10.82**	**1.52**